Sun, Y., Liu, Z., Liang, Y. and Zhao, O. (2019) Experimental and numerical investigations of hot-rolled austenitic stainless steel equal-leg angle sections. *Thin-Walled Structures*, 144, 106225.
(doi: 10.1016/j.tws.2019.106225)

Experimental and numerical investigations of hot-rolled austenitic stainless steel equal-leg angle sections

Yao Sun [a], Zhanke Liu [b], Yating Liang [c], Ou Zhao [*a]

[a] School of Civil and Environmental Engineering, Nanyang Technological University, Singapore

[b] School of Civil Engineering and Mechanics, Lanzhou University, Lanzhou, China

[c] School of Engineering, University of Glasgow, Glasgow, UK

[*] Corresponding author, Phone: +65 6790 6934

Email: ou.zhao@ntu.edu.sg

Abstract: The present paper reports a thorough experimental and numerical study on the cross-section behaviour of hot-rolled austenitic stainless steel equal-leg angle section structural members. The experimental programme was performed on a total of five different angle sections, and involved ten stub column tests and ten laterally restrained 4-point bending tests about the cross-section geometric axes (parallel to the angle legs), together with measurements on material properties and initial local geometric imperfections. The testing programme was followed by a systematic finite element simulation programme, where the developed numerical models were firstly validated against the experimentally derived results and then employed to carry out parametric studies for the purpose of generating further structural performance data over a broader range of cross-section dimensions. The numerically derived results were then employed together with the test data to assess the accuracy of the established design rules for hot-rolled austenitic stainless steel equal-leg angle section stub columns and beams given in the European code. The results of the assessment revealed an overly high level of conservatism and scatter of the European code in predicting cross-section capacities of hot-rolled austenitic stainless steel equal-leg angle section stub columns and beams, which can be mainly attributed to the neglect of the beneficial material strain hardening. The continuous strength method (CSM) is a well-established design approach, taking due account of material strain hardening in the determination of cross-section resistances, and has been recently extended to cover the design of mono-symmetric and asymmetric stainless steel open sections in compression and bending about an axis that is not one of symmetry. The CSM was assessed against the experimental and numerical results on hot-rolled austenitic stainless steel equal-leg angle section stub columns and laterally restrained beams, and shown to result in substantially more precise and consistent cross-section capacity predictions than the European code.

Keywords: Austenitic stainless steel; Continuous strength method; Cross-section behaviour European code; Hot-rolled equal-leg angle sections; Stub column tests; Geometric axis bending tests; Numerical simulation

1. Introduction

Unprecedented emphasis has been placed on the use of sustainable construction material in civil engineering applications over the past two decades. Compared to carbon steel, stainless steel exhibits exceptional resistance against corrosion as well as excellent durability, resulting in significantly reduced maintenance cost during its service life and thus life-cycle cost effectiveness, and is 100% recyclable after use. The sustainable nature and attractive appearance, together with the desirable mechanical properties, including high strength and ductility, popularise the use of stainless steel as a construction material in civil and offshore engineering. Angle section members are extensively utilised as lateral bracing components (undertaking compression and tension forces) in steel frames, chords (transferring compression and tension forces) in transmission towers and windposts (carrying bending moments about the member geometric axes) in masonry walls. Although extensive studies have been conducted on different types of carbon steel equal- and unequal-leg angle section structural components [1–9], research into their stainless steel counterparts remained scarce, with a brief summary provided herein. Kuwamura [10] conducted stub column tests on cold-formed austenitic stainless steel equal-leg angle sections to study their cross-section compression resistances. The local buckling behaviour of laser-welded austenitic stainless steel equal-leg and unequal-leg angle section beams in bending about their geometric axes (parallel to the angle legs) was experimentally investigated by Theofanous et al. [11]. Liang et al. [12], de Menezes et al. [13] and Zhang et al. [14] carried out tests and numerical modelling on fixed-ended austenitic stainless steel equal-leg angle section intermediate columns, to investigate their flexural-torsional buckling behaviour and strengths subject to compression.

To expand the experimental and numerical data pool on stainless steel angle section structural members, a systematic testing and numerical modelling programme is underway at Nanyang Technological University, and as part of this programme, experimental and numerical investigations into the cross-section behaviour of hot-rolled austenitic stainless steel equal-leg angle section stub columns and laterally restrained beams were preformed and reported in the present paper. The testing programme was performed on five hot-rolled equal-leg angle sections made of three austenitic stainless steel grades, and involved material testing, initial imperfection measurements, ten stub column tests, and ten laterally restrained beam tests about the cross-section geometric axes. The testing programme was followed by a finite element simulation programme, where numerical models were firstly developed and validated against the test data, and then adopted to conduct parametric studies to generate further numerical results to supplement the experimental data pool over a wider range of cross-section dimensions. The obtained experimental and numerical results were then adopted to evaluate the accuracy of the design rules for hot-rolled austenitic stainless steel equal-leg angle section stub columns and laterally restrained beams, given in the European code EN 1993-1-4 [15] and the continuous strength method [16–18].

2. Experimental study

2.1. General

A thorough testing programme was firstly conducted to study the cross-section behaviour and load-carrying capacities of hot-rolled austenitic stainless steel equal-leg angle sections subject to compression and bending about the geometric axes. The testing programme involved material tensile coupon tests, initial local imperfection measurements, ten stub column tests, and ten laterally restrained beam tests about the cross-section geometric axes. Five hot-rolled austenitic stainless steel equal-angle sections were considered in the structural testing: A 80×10 of grades EN 1.4307, EN 1.4404 and EN 1.4571, A 100×10 of grade EN 1.4307 and A 100×8 of grade EN 1.4571, of which the cross-section identifiers are denoted as A1, A2, A3, A4 and A5, respectively. The labelling system for angle section specimens starts with the cross-section identifier, followed by a letter ‘S’ or ‘B’ (indicating a stub column or a beam), and ends with a number ‘1’ or ‘2’ (utilised to distinguish the two nominally identical specimens for each type of testing), e.g., A3-S1 represents an A 80×10 stub column specimen made of grade EN 1.4571 stainless steel.

2.2. Material tensile coupon tests

Prior to stub column and laterally restrained beam tests, material testing was carried out. The setup and procedures of the material tensile coupon tests were fully reported in Liang et al. [12], with only a brief summary given herein. For each of the five examined hot-rolled austenitic stainless steel equal-leg angle sections, two coupons were cut along the centrelines of both legs (see Fig. 1), and tested using a Schenck 250 kN hydraulic testing machine under displacement control, with the resulting strain rate being in conformity to the specific requirements set out in EN ISO 6892-1 [19]. Table 1 summaries the average measured material properties for each angle section, including the Young’s modulus E, the 0.2% and 1.0% proof stresses $\sigma_{0.2}$ and $\sigma_{1.0}$, the ultimate tensile stress σ_u, the strains at the ultimate tensile stress and at fracture (ε_u and ε_f, respectively) and the coefficients adopted in the Ramberg–Osgood material model for nonlinear metallic materials n and $n'_{0.2,1.0}$ [20–24].

2.3. Initial local geometric imperfection measurements

Initial geometric imperfections were introduced into stainless steel (hot-rolled, cold-formed and welded) members during the manufacturing process, and may affect their structural performance. The focus of the present study is on the cross-section behaviour of austenitic stainless steel equal-leg angle section stub columns and laterally restrained beams, of which the (schematic) failure modes are illustrated in Figs 2(a) and 2(b), respectively; thus the initial local geometric imperfection of each specimen was measured, following the procedures recommended by Schafer and Peköz [25]. Figs 2(c) depicts the test rig for the measurements of initial local geometric imperfections of the specimens, in which T-slot clamps are utilised to clamp the angle section specimen on a milling table, and two pairs of linear variable displacement transducers (LVDTs) are placed at both legs of the angle section specimen to measure the local deviations along four representative longitudinal lines. For each angle leg, the initial local geometric imperfection amplitudes were taken as the deviations from a best-fitting linear regression surface to the dataset measured from the two LVDTs (LVDTs 1-1 and 1-2 or LVDTs 2-1 and 2-2) [11,26–28], with the maximum deviation denoted as $\omega_{\mathrm{max},1}$ (or $\omega_{\mathrm{max},2}$), while the initial local geometric imperfection of the angle section specimen ω_0 is defined as the maximum of $\omega_{\mathrm{max},1}$ and $\omega_{\mathrm{max},2}$. Table 2 reports $\omega_{\mathrm{max},1}$, $\omega_{\mathrm{max},2}$ and ω_0 for each of the tested angle section stub columns and laterally restrained beams.

2.4. Stub column tests

Two repeated stub column tests were conducted on each of the five examined austenitic stainless steel equal-leg angle sections, to study their cross-section behaviour and compressive capacities. The nominal length of each angle section stub column specimen was taken as three times the leg width [29]. Table 2 presents the measured geometric dimensions as well as the initial local imperfection amplitudes ω_0 for the angle section stub column specimens, where L is the specimen length, and b and t are respectively the leg width and thickness of the angle section. Fig. 3 displays the stub column test rig, where a pair of anchor devices is used at both ends of the angle section specimen to prevent any possibility of end rotations about both the principal axes as well as torsional rotation and achieve the fixed-ended boundary condition, two LVDTs are placed at the loaded end of the specimen to capture the end shortening of the stub column, and two strain gauges are affixed along the centrelines of the outer surfaces of both angle legs at mid-height to record the axial compressive strains. It is worth noting that the behaviour and strengths of equal-leg angle section columns are dependent on the boundary conditions. There are three types of boundary conditions, namely fixed-ended boundary condition, pin-ended boundary condition provided by knife-edge (i.e. pinned with respect to minor-axis flexure and fixed with respect to major-axis flexure, torsion and warping) and pin-ended boundary condition provided by spherical bearing (i.e. pinned with respect to major-axis and minor-axis flexure and fixed with respect to torsion and warping). However, for angle section stub columns with short member lengths, the influence of boundary conditions on their structural performance and load-carrying capacities is negligible. In the present study, fixed-ended boundary condition was employed for all the stub column tests. All the stub columns were concentrically compressed by an Instron 2000 kN hydraulic testing machine, with the loading rate of 0.2 mm/min. The readings of the LVDTs in the stub column tests comprise not only the axial end shortening of the specimen but also the deformation of the end platens of the hydraulic testing machine (which is approximately elastic). The LVDT readings were then modified, on the basis of the strain gauge values and in accordance with the procedures given in [30], in order to derive the actual end shortenings of the stub column specimens. This was achieved by assuming that the end platen deformation was proportional to the applied load and shifting the load–end shortening curves derived from the LVDTs such that the initial slope matched that obtained from the strain gauges. Fig. 4 shows the modified (actual) load–end shortening curves for the ten hot-rolled austenitic stainless steel equal-leg angle section stub column specimens, with the key derived experimental results displayed in Table 3, where N_u is the ultimate load, δ_u is the axial end shortening corresponding to the ultimate load, and $N_u/(A\sigma_{0.2})$ is the ultimate to cross-section yield load ratio, where A is the gross area of the angle section. All the tested hot-rolled austenitic stainless steel equal-leg angle section stub columns display flexural-torsional buckling mode, although the torsional deformation is much more visible than the major-axis flexure; a typical failed specimen A3-S1 is shown in Fig. 5.

2.5. Laterally restrained beam tests about the cross-section geometric axes

A total of ten laterally restrained beam tests were conducted on the five studied hot-rolled austenitic stainless steel equal-leg angle sections in the four-point bending configuration, aiming to investigate their in-plane behaviour and strengths subjected to constant bending moment about the cross-section geometric axes. Note that there are two orientations associated with the angle section beams bent about the cross-section geometric axes, as depicted in Fig. 6, in which the 'L' orientation bending induces tension in the bottom (horizontal) leg, while bending in the 'reverse L' orientation results in compression in the top (horizontal) leg, which is more critical; the present laterally restrained beam tests on equal-leg angle sections were thus performed about their geometric axes in the 'reverse L' orientation. For each angle section, two nominally identical beams were bolted to the same set of 75 mm thick spacer plates and further stiffened by G-clamps at the two loading points and supports to form compound sections at these locations, as schematically depicted in Fig. 7, and then tested together. In comparison with single-angle beams in bending about the geometric axes in the 'reverse L' orientation, which are susceptible to lateral torsional buckling, double-angle beams with compound sections at the loading points and supports possess significantly enhanced overall member out-of-plane torsional stiffnesses, thus eliminating the possibility of lateral torsional buckling. Fig. 8 displays the test rig for laterally restrained (double-angle) beams in bending about the geometric axes, where two steel rollers are positioned at a distance of 50 mm from the ends of the paired angle section beams, to provide simply-supported boundary conditions, a spreader beam is used, together with another two steel rollers located at third-points of the beam flexural span, for the purpose of application of loading, and three string potentiometers are positioned at the two loading points and mid-span to obtain the respective vertical deflections at these locations. The member lengths of all the ten tested austenitic stainless steel equal-leg angle section beams were equal to 1600 mm, leading to the flexural span lengths of 1500 mm and the lengths between the two loading points equal to 500 mm. Displacement-control loading scheme was also utilised for the laterally restrained beam tests at a constant rate of 2 mm/min.

The normalised moment–curvature curves for the tested hot-rolled austenitic stainless steel equal-leg angle section beams in bending about the geometric axes in the 'reverse L' orientation are shown in Fig. 9, where the curvature κ is calculated from Eq. (1), in which D_L and D_M are respectively the measured vertical deflections at the loading points and mid-span, and L_m=500 mm is the distance between the loading points. The key results derived from the laterally restrained hot-rolled austenitic stainless steel equal-leg angle section beam tests are given in Table 4, including the failure moment M_u, the M_u/M_{pl} and M_u/M_{el} ratios, in which $M_{pl}=W_{pl}\sigma_{0.2}$ and $M_{el}=W_{el}\sigma_{0.2}$ are the cross-section plastic and elastic moment resistances about the geometric axes, respectively; note that the plastic and elastic section moduli W_{pl} and W_{el} are respectively calculated about the plastic neutral axis (PNA) and elastic neutral axis (ENA) of the angle section (see Fig. 6), and the rotation capacity of the beam R, as calculated from Eq. (2), where $\kappa_{pl}=M_{pl}/EI$ is defined as the elastic curvature corresponding to the plastic moment M_{pl}, in which I is the second moment of area with respect to the ENA, and κ_u is the curvature at which the falling branch of the moment–curvature curve drops back to M_{pl}. All the tested laterally restrained hot-rolled austenitic stainless steel equal-leg angle section beams underwent pronounced in-plane deformation and failure, with a typical failed specimen A1-B1 displayed in Fig. 10.

$$\kappa=\frac{8\left(D_M-D_L\right)}{4\left(D_M-D_L\right)^2+L_m^2} \tag{1}$$

$$R = \frac{\kappa_{\mathrm{u}}}{\kappa_{\mathrm{pl}}} - 1 \quad (2)$$

3. Numerical simulation study

3.1. General

In parallel with the structural testing conducted in Section 2, a systematic numerical simulation study was carried, using the nonlinear finite element software ABAQUS [31], and fully reported in this section. Finite element (FE) models were firstly developed to simulate the hot-rolled austenitic stainless steel equal-leg angle section stub column and laterally restrained beam tests, and then utilised to conduct parametric studies to derive additional numerical data over a broader spectrum of cross-section dimensions.

3.2. Development of finite element models

The shell element S4R [31], having been successfully and extensively utilised in previous numerical simulations of stainless steel open (angle, channel, and I-) section structural members [12,14,18,32–35], was also adopted herein. The element size was selected upon a mesh sensitivity study examining a range of element sizes from 0.5t to 3t; it was found that an element size equal to the angle section thickness can not only provide accurate numerical simulation results but also offer satisfactory computational efficiency. Therefore, a uniform mesh with the size equal to the material thickness along both the longitudinal direction of the member and the centreline of the cross-section was assigned to each of the angle section stub column and beam FE models. Regarding the material modelling of stainless steel, the plastic material model given in ABAQUS [31] required the inputted material properties to be specified in the form of true stress and true plastic strain for the used S4R shell element. Therefore, the measured engineering stress−strain curves were firstly converted into the true stress−true plastic strain responses and then incorporated into ABAQUS [31]. The tested stainless steel equal-leg angle section specimens were fabricated by hot-rolling, which introduces relatively low levels of membrane residual stresses, compared to welding [36–38]. On this basis, and coupled with the fact that the studied cross-section compression behaviour and in-plane bending response are both largely insensitive to membrane residual stresses [39–41], explicit modelling of membrane residual stresses in the numerical models was deemed unnecessary. Suitable boundary conditions were then applied to the developed FE models to mimic the boundary conditions utilised in the testing. For each stub column FE model, the two end sections were fully restrained except for longitudinal translation at one end, to achieve the same fixed-ended boundary condition employed in the stub column tests. For each beam FE model, the two end sections were coupled with two reference points positioned at the tips of the vertical angle legs, with one allowed for longitudinal translation as well as rotation about the cross-section geometric axis and the other one only allowed to rotate about the same geometric axis, while the two cross-sections at the loading points were coupled with another two reference points located at the mid-points of the horizontal angle legs, allowed to have translations along both the vertical and longitudinal directions and rotation about the same geometric axis as the two end reference points; this replicates the simply-supported boundary condition and four-point bending configuration adopted in the laterally restrained beam experiments. Initial local geometric imperfections were included into the stub column and beam numerical models in the form of the respective lowest elastic buckling mode shapes [42–46], factored by a total of five different imperfection amplitudes, including the measured value ω_0 and 1/10, 1/20, 1/50 and 1/100 of the material thicknesses; this enables the sensitivity of the developed stub column and beam FE models to the local geometric imperfection amplitudes to be evaluated.

3.3. Validation of finite element models

Upon development of the hot-rolled austenitic stainless steel equal-leg angle section stub column and beam FE models, nonlinear Riks analysis [31] was carried out to derive the numerical ultimate strengths, load–deformation responses and failure modes, which were then compared against the corresponding experimentally observed results, allowing the accuracy of the developed FE models to be evaluated. Tables 5 and 6 present the ratios of the FE to test ultimate loads and moments for the tested hot-rolled austenitic stainless steel equal-leg angle section stub columns and beams, respectively. It was observed that all the five considered initial local imperfection levels generally yield fairly accurate predictions of the experimental failure loads (or moments), with the best agreement obtained when the imperfection value of $t/50$ was utilised in the FE models. Figs 11 and 12 depict the test and FE load–deformation histories for the typical stub column and laterally restrained beam specimens, respectively, showing good agreement; it is also worth noting that incorporation of a larger local geometric imperfection amplitude into the FE model generally leads to lower ultimate load and deformation as well as steeper post-ultimate load–deformation response, but with no significant effect on the initial stiffness of the load–deformation curve. The experimental failure modes were also found to be well replicated by their numerical counterparts, as illustrated in Figs 5 and 10. In sum, the developed FE models have been proven to be capable of precisely simulating the hot-rolled austenitic stainless steel equal-leg angle section stub column and laterally restrained beam tests.

3.4. Parametric studies

Parametric studies were performed in this section, based on the validated FE models, to generate additional numerical data over a wider range of cross-section dimensions. In the present parametric studies, the material stress–strain response measured from the tensile coupon test on angle section A 80×10 of grade EN 1.4404 (i.e. angle section A2) was utilised, while the amplitude of $t/50$ was adopted to scale the initial local geometric imperfection pattern (in the form of the lowest elastic buckling mode shape). With regards to the geometric dimensions of the modelled equal-leg angle sections, the leg widths of the beam models were fixed at 100 mm, while the leg widths were equal to 50 mm, 75 mm and 100 mm for the modelled stub columns, with the material thicknesses varying from 2.5 mm to 16 mm, resulting in a broad range of cross-section slendernesses being examined. The lengths of the stub column numerical models were taken as three times the leg widths, while the lengths of the flexural spans of the modelled beams were equal to 1500 mm, with concentrated loads applied at third-points of the flexural spans. In total, 98 numerical parametric study results were generated for hot-rolled austenitic stainless steel equal-leg angle section stub columns and laterally restrained beams.

4. Evaluation of existing design approaches

4.1. General

In this section, the experimental and numerical results were utilised to assess the accuracy of the current design rules for hot-rolled austenitic stainless steel equal-leg angle section stub columns and laterally restrained beams, as given in the established Eurocode EN 1993-1-4 [15] and novel continuous strength method (CSM) [16–18]. For the considered equal-leg angle section stub columns and laterally restrained beams, the unfactored design compression and bending capacities ($N_{u,pred}$ and $M_{u,pred}$, respectively) were calculated from both of the two design approaches, based on all the partial safety factors set to be equal to unity, and then compared against the corresponding experimental (and FE) ultimate loads and bending moments (N_u and M_u, respectively), with the mean ratios of $N_u/N_{u,pred}$ and $M_u/M_{u,pred}$ shown in Table 7.

4.2. European code EN 1993-1-4 (EC3)

4.2.1. General

The design rules for stainless steel angle section structural members failing by local buckling, as given in EN 1993-1-4 [15], were developed on the basis of the conventional cross-section classification framework, together with an elastic, perfectly-plastic material model. Four cross-section classes are specified in the Eurocode EN 1993-1-4 [15]: Class 1 and 2 (plastic) sections are capable of achieving the plastic moment capacities (M_{pl}) and yield loads ($A\sigma_{0.2}$) when subjected to bending and compression, respectively, Class 3 (elastic) sections under bending and compression can attain the elastic moment capacities (M_{el}) and yield loads ($A\sigma_{0.2}$), and Class 4 (slender) sections fail prior to the achievement of the material yield (0.2% proof) stress, limiting the cross-section resistances to the effective bending and compression resistances (M_{eff} and N_{eff}). The classification of an angle section is made by comparing the width-to-thickness ratios of both legs against the corresponding codified slenderness limits, which are dependent on the applied loadings on the angle legs. Note that the current Eurocode EN 1993-1-4 [15] only specifies the Class 3 slenderness limit for hot-rolled stainless steel angle sections under compression, where both of the two legs are subjected to the uniform compressive stress, but provides no provisions on the classification limits for hot-rolled stainless steel angle sections subjected to other loading cases (e.g., bending and combined compression and bending), in which the stress distributions in the two legs are different. In the following Section 4.2.2, the accuracy of the EC3 Class 3 slenderness limits for hot-rolled stainless steel angle sections under compression was evaluated, and the applicability of the corresponding EC3 slenderness limits for welded and cold-formed stainless steel angle sections in bending to their hot-rolled counterparts was also examined, while assessment of the EC3 compression and bending moment resistance predictions for hot-rolled austenitic stainless steel equal-leg angle sections was conducted in Section 4.2.3.

4.2.2. Cross-section classification limits

For hot-rolled stainless steel angle sections in compression, the current EN 1993-1-4 [15] defines non-slender (Class 1, 2 and 3) cross-sections as those with the geometric dimensions satisfying $b/(t\varepsilon)\leq 15$ and $0.5(b+h)/(t\varepsilon)\leq 11.5$, in which b and h are respectively the widths of the longer and shorter legs of the angle section, and $\varepsilon=[(235/\sigma_{0.2})(E/210000)]^{0.5}$, leading to the EC3 Class 3 slenderness limit of $b/(t\varepsilon)=11.5$ for equal-leg stainless steel angle sections (with $b=h$) in compression. The experimental and FE ultimate loads of hot-rolled austenitic stainless steel equal-leg angle section stub columns are normalised by the corresponding cross-section yield loads, and plotted against the $b/(t\varepsilon)$ ratios of the angle legs, together with the EC3 Class 3 slenderness limit for stainless steel equal-leg angle sections in compression ($b/(t\varepsilon)=11.5$), as shown in Fig. 13. The results of the comparison generally revealed that the EC3 Class 3 slenderness limit is safe but conservative for hot-rolled austenitic stainless steel equal-leg angle sections subjected to compression.

The current EN 1993-1-4 [15] provides no provisions on the classification limits for hot-rolled stainless steel angle sections in bending, in which the stress distributions in the two legs are different, and the applicability of the corresponding EC3 slenderness limits for welded and cold-formed stainless steel angle sections in bending to their hot-rolled counterparts was assessed. For an equal-leg angle section beam bent about the geometric axis in the 'reverse L' direction, the vertical leg is subjected to a stress gradient while the horizontal leg is under uniform compressive stress and thus more critical. The test (and numerical) ultimate moments of hot-rolled austenitic stainless steel equal-leg angle section beams are normalised by the corresponding elastic and plastic moment capacities, respectively, and then plotted against the $b/(t\varepsilon)$ ratios of the critical horizontal legs in Figs 14 and 15, together with the EC3 Class 3 and 2 slenderness limits for welded and cold-formed stainless steel outstand elements in compression ($b/(t\varepsilon)$=14 and $b/(t\varepsilon)$=10, respectively). The results of the comparison generally indicated that the current EN 1993-1-4 Class 3 and 2 slenderness limits for welded and cold-formed stainless steel outstand elements in compression are applicable to their hot-rolled counterparts, but are unduly conservative.

4.2.3. Assessment of EC3 compression and bending moment resistance predictions

The EC3 predictions of cross-section capacities for hot-rolled stainless steel equal-leg angle sections under compression and bending were assessed through comparisons against the stub column and beam test (and FE) results. The current Eurocode EN 1993-1-4 [15] specifies the plastic (M_{pl}), elastic (M_{el}) and effective (M_{eff}) moment capacities as the design cross-section bending moment resistances for Class 1 (and 2), Class 3, and Class 4 stainless steel angle sections, respectively, and prescribes the use of the cross-section yield loads ($A\sigma_{0.2}$) and effective compression resistances (N_{eff}) as the design compression capacities for non-slender (Class 1, 2 and 3) and slender (Class 4) stainless steel angle sections, respectively. Note that the EN 1993-1-4 effective width formulations were originated from stainless steel plates, regardless of the cross-section types (cold-formed, welded and hot-rolled), and thus theoretically suitable for not only cold-formed and welded stainless sections but also their hot-rolled counterparts. The applicability of the effective width formulations to hot-rolled slender austenitic stainless steel equal-leg angle sections in compression and bending was evaluated herein by comparing the effective cross-section resistances against the corresponding experimental and numerical results.

The failure loads and moments, obtained from structural testing as well as numerical modelling on hot-rolled austenitic stainless steel equal-leg angle section stub columns and laterally restrained beams, were normalised by the corresponding EC3 design cross-section resistances, and then plotted against the $b/(t\varepsilon)$ ratios of the critical angle legs, as depicted in Fig. 16, while Table 7 reports the mean test (or numerical) to EC3 predicted ultimate load and moment ratios $N_u/N_{u,EC3}$ and $M_u/M_{u,EC3}$, respectively. The results of both the graphic and quantitative evaluations showed that EN 1993-1-4 [15] results in unduly scattered and conservative predictions of cross-section capacities for hot-rolled stainless steel equal-leg angle section structural members, principally attributed to the adoption of an elastic, perfectly plastic material model without accounting for material strain hardening of stainless steel in the design.

It is worth noting that for slender (Class 4) angle section bent about the geometric axis in the 'reverse L' direction, where the neutral axis is closer to the extreme compressive fibre, although the compressive strains are less than yield strain, the tensile strains can be considerably greater than the yield strain (see Fig. 17), indicating that the tensile portions of slender angle sections in bending can also benefit from strain hardening, owing to which Class 4 angle sections may even attain failure moments greater than the cross-section plastic moment capacities (for example, the experimental to plastic moment capacity ratios for the tested Class 4 hot-rolled austenitic stainless steel equal-leg angle section beam specimens A5-B1 and A5-B2 are equal to 1.12). However, the established EN 1993-1-4 [15] ignores this favourable strain hardening effect associated with the tensile portions of slender stainless steel angle sections bent about the geometric axes in the 'reverse L' direction, and limits the cross-section bending moment capacities to the effective moment resistances, leading to an excessively high level of deign conservatism.

4.3. Continuous strength method (CSM)

Continuous strength method (CSM) [16–18] is a well-established design approach, taking due account of material strain hardening in the predictions of cross-section capacities. In comparison with the EC3 local buckling design rules [15], which were developed on the basis of the cross-section classification framework and an elastic, perfectly plastic material model, the CSM [16–18] relates the resistance of a cross-section to its deformation capacity and further utilises an elastic, linear hardening material model to consider the beneficial effect of strain hardening and achieve the design stress greater than the material yield (0.2% proof) stress. The application scope of the CSM has been recently extended from doubly symmetric I-sections and tubular sections to non-doubly symmetric sections [18], including mono-symmetric T- and channel sections and asymmetric angle sections. In this section, the accuracy of the CSM [16–18] to the design of hot-rolled austenitic stainless steel equal-leg angle sections in bending and in compression was assessed.

The first step toward the use of the CSM [16–18] is the determination of the cross-section deformation capacity, expressed in terms of the limiting (maximum attainable) compressive strain ε_{csm}; this can be achieved through utilising the CSM 'base curve', which defines the relationship between the limiting compressive strain ratio $\varepsilon_{csm}/\varepsilon_y$ and cross-section slenderness $\bar{\lambda}_p = \sqrt{\sigma_{0.2}/\sigma_{cr}}$, as given by Eq. (3), in which ε_y=$\sigma_{0.2}/E$ is the yield strain, and σ_{cr} is the elastic critical buckling stress of the examined angle section under the applied loading (i.e. compression or bending about the cross-section geometric axis in the 'reverse L' orientation), and may be derived by utilising the finite strip software CUFSM [47]. Note that the cross-section slenderness limit of $\bar{\lambda}_p = 0.68$, where the limiting compressive strain ratio $\varepsilon_{csm}/\varepsilon_y$ is equal to unity, distinguishes non-slender sections from their slender counterparts.

$$\frac{\varepsilon_{csm}}{\varepsilon_y} = \begin{cases} \dfrac{0.25}{\bar{\lambda}_p^{3.6}} \text{ but} \le \min\left(15, \dfrac{C_1\varepsilon_u}{\varepsilon_y}\right) & \text{for } \bar{\lambda}_p \le 0.68 \\ \left(1 - \dfrac{0.222}{\bar{\lambda}_p^{1.05}}\right) \cdot \dfrac{1}{\bar{\lambda}_p^{1.05}} & \text{for } \bar{\lambda}_p > 0.68 \end{cases} \quad (3)$$

In comparison with the elastic, perfectly plastic material model employed in the Eurocode EN 1993-1-4 [15], a novel elastic, linear strain hardening material model, featuring four material parameters (C_1, C_2, C_3 and C_4) and shown in Fig. 18, is utilised in the CSM [16–18], allowing for achievement of the design failure stresses greater than the 0.2% proof stress for cross-sections with limiting compressive strains greater than the yield strain. The material parameter C_1 is employed in Eq. (3) to define a cut-off stain for the purpose of preventing over-predictions of the CSM design failure stresses, while the parameter C_2 is employed in Eq. (4) for defining the strain hardening slope E_{sh} of the CSM material model. The parameters C_3 and C_4 are used for predicting the material failure strain $\varepsilon_u = C_3(1-\sigma_{0.2}/\sigma_u)+C_4$. The values of the four material parameters C_1, C_2, C_3 and C_4 are respectively equal to 0.1, 0.16, 1.0 and 0.0 for austenitic stainless steel [48].

$$E_{sh} = \frac{\sigma_u - \sigma_{0.2}}{C_2\varepsilon_u - \varepsilon_y} \tag{4}$$

The CSM design failure stress corresponding to the limiting compressive strain can then be determined, on the basis of the CSM elastic, linear strain hardening material model, as given by Eq. (5). Note that for non-slender angle sections with the limiting compressive strains greater than the material yield strain (i.e. limiting compressive strain ratios greater than unity), the derived CSM design failure stresses exceed the 0.2% proof stress, allowing for the beneficial strain hardening effect to be accounted for, while for slender angle sections with the limiting strain ratios less than unity, the derived CSM design failure stresses less than the 0.2% proof stress reflect the earlier occurrence of local buckling. The CSM cross-section capacity in compression is then given as the product of the CSM design failure stress and the gross area of the cross-section, as shown in Eq. (6).

$$\sigma_{csm} = \begin{cases} \sigma_{0.2}\varepsilon_{csm}/\varepsilon_y & \text{for } \varepsilon_{csm} < \varepsilon_y \\ \sigma_{0.2} + E_{sh}\left(\varepsilon_{csm} - \varepsilon_y\right) & \text{for } \varepsilon_{csm} \geq \varepsilon_y \end{cases} \tag{5}$$

$$N_{csm} = A\sigma_{csm} \tag{6}$$

For an angle section bent about the geometric axis in the 'reverse L' orientation, the limiting compressive strain $\varepsilon_{csm,c}$ is calculated from the base curve defined by Eq. (3), while the limiting tensile strain $\varepsilon_{csm,t}$ is derived from Eq. (7), assuming that the strain distribution is linear-varying throughout the depth of the angle section, as depicted in Fig. 19, where b is the overall height of the angle section, and y_c is the distance from the outer compressive fibre to the CSM design neutral axis, which is taken as the ENA for relatively slender angle sections with cross-section slenderness $\bar{\lambda}_p > 0.6$, but assumed to be located at the mid-point between the ENA and PNA for those stocky angle sections with $\bar{\lambda}_p \leq 0.6$. The CSM stress distribution for an angle section bent about the geometric axis in the 'reverse L' orientation can then be derived, based on the CSM elastic, linear strain hardening material model. If the CSM design strain $\varepsilon_{csm,d}$, defined as the maximum of the limiting compressive and tensile strains ($\varepsilon_{csm,c}$ and $\varepsilon_{csm,t}$), is less than the yield strain ε_y, the CSM design stress distribution throughout the angle section depth is elastic as well as linear-varying (see Fig. 19(a)), with no benefit arising from strain hardening. In this scenario, the CSM capacities for angle sections bent about the geometric axes are given as the products of the cross-section elastic moment capacities M_{el}=$W_{el}\sigma_{0.2}$ and the design strain ratios $\varepsilon_{csm,d}/\varepsilon_y$, as shown in Eq. (8). If the CSM design strain $\varepsilon_{csm,d}$ exceeds ε_y, which indicates that at least one of the compressive and tensile portions of the angle section can benefit from strain hardening (see Figs 19(b) and 19(c)), the CSM bending moment capacity was firstly derived by integrating the CSM design stress over the angle section depth, and then transformed into a simplified formulation [18], as given by Eq. (9), in which α is the CSM bending parameter and equal to 1.5 for equal-leg angle sections bent about the geometric axes. As highlighted in Section 4.2.3, the tensile portions of slender (Class 4) angle sections bent about the geometric axes in the 'reverse L' direction can still benefit from material strain hardening, as illustrated in Fig. 19(b). This favourable strain hardening effect associated with the tensile portions of slender angle sections is taken due account of in the CSM [18].

$$\varepsilon_{\mathrm{csm,t}} = \frac{\varepsilon_{\mathrm{csm,c}}\left(b - y_{\mathrm{c}}\right)}{y_{\mathrm{c}}} \quad \text{but} \frac{\varepsilon_{\mathrm{csm,t}}}{\varepsilon_{\mathrm{y}}} \le \min\left(15, \frac{C_1 \varepsilon_{\mathrm{u}}}{\varepsilon_{\mathrm{y}}}\right) \tag{7}$$

$$M_{\mathrm{csm}} = W_{\mathrm{el}} \sigma_{0.2} \frac{\varepsilon_{\mathrm{csm,d}}}{\varepsilon_{\mathrm{y}}} \quad \text{for } \varepsilon_{\mathrm{csm,d}} < \varepsilon_{\mathrm{y}} \tag{8}$$

$$M_{\mathrm{csm}} = W_{\mathrm{pl}} \sigma_{0.2} \left[1 + \frac{E_{\mathrm{sh}}}{E} \frac{W_{\mathrm{el}}}{W_{\mathrm{pl}}} \left(\frac{\varepsilon_{\mathrm{csm,d}}}{\varepsilon_{\mathrm{y}}} - 1\right) - \left(1 - \frac{W_{\mathrm{el}}}{W_{\mathrm{pl}}}\right) \Big/ \left(\frac{\varepsilon_{\mathrm{csm,d}}}{\varepsilon_{\mathrm{y}}}\right)^{\alpha}\right] \quad \text{for } \varepsilon_{\mathrm{csm,d}} \ge \varepsilon_{\mathrm{y}} \tag{9}$$

The stub column and laterally restrained beam test (and FE) results on hot-rolled austenitic stainless steel equal-leg angle sections were compared with the CSM cross-section compression and bending capacities, with the mean ratios of $N_{\mathrm{u}}/N_{\mathrm{u,csm}}$ and $M_{\mathrm{u}}/M_{\mathrm{u,csm}}$ reported in Table 7. The comparison results generally indicated that the CSM [16–18] leads to substantially more precise and consistent predicted capacities for hot-rolled austenitic stainless steel equal-leg angle sections than the existing Eurocode EN 1993-1-4 [15], owing to the consideration of strain hardening, as also evident in Fig. 20, where the ratios of the test (or numerical) ultimate loads and moments to the predicted resistances determined from both the EN 1993-1-4 [15] and CSM [16–18] are plotted against the cross-section slendernesses.

Numerical assessment of the CSM [16–18] was also carried out, on the basis of the experimental data only. The mean ratios of $N_{\mathrm{u}}N_{\mathrm{u,csm}}$ and $M_{\mathrm{u}}/M_{\mathrm{u,csm}}$, as reported in Tables 3 and 4, are equal to 1.07 and 1.20, respectively, with the coefficients of variation (COVs) of 0.04 and 0.05, indicating a higher level of accuracy and consistency in the prediction of cross-section capacities for hot-rolled austenitic stainless steel equal-leg angle sections than the

Eurocode EN 1993-1-4 [15], which leads to the mean ratios of $N_u/N_{u,EC3}$ and $M_u/M_{u,EC3}$ equal to 1.13 and 2.00, with COVs of 0.07 and 0.18, respectively.

5. Conclusions

An experimental and numerical investigation of the cross-section behaviour of hot-rolled austenitic stainless steel equal-leg angle section stub columns and laterally restrained beams has been reported. The testing programme involved material testing, initial geometric imperfection measurements, ten stub column tests and ten laterally restrained beam tests about the cross-section geometric axes. Following the laboratory testing, a finite element simulation investigation was performed, where the developed numerical models were firstly validated against the test results and then used to conduct parametric studies to expand the experimental data pool over a broader range of cross-section slendernesses. The obtained test and FE data were employed to evaluate the accuracy of the relevant design provisions established in the current EN 1993-1-4 [15]. The results of the evaluation revealed that EN 1993-1-4 [15] leads to both conservative and scattered compression and bending moment capacity predictions for hot-rolled austenitic stainless steel equal-leg angle section stub columns and laterally restrained beams, mainly owing to the neglect of the beneficial effect of material strain hardening of austenitic stainless steel. The continuous strength method (CSM) [16–18] is a deformation-based design method, accounting for strain hardening in predicting cross-section resistances. The CSM [16–18] was evaluated against the derived experimental and FE results on hot-rolled austenitic stainless steel equal-leg angle section stub columns and laterally restrained beams, and shown to lead to substantially improved cross-section resistance predictions over the current EN 1993-1-4 [15].

Acknowledgements

The authors would like to thank Acerinox, S.A. for sponsoring hot-rolled austenitic stainless steel equal-leg angle sections and to Mr. Cheng Hoon Tui and Mr. Siew Pheng Choi for their assistances in the tests. The financial support from NTU Research Scholarship is also acknowledged.

References

[1] S. Kitipornchai, H.W. Lee, Inelastic experiments on angle and tee struts, J. Constr. Steel Res. 6 (3) (1986) 219–236.

[2] M.K.S. Madugula, T. Kojima, Y. Kajita, M. Ohama, Geometric axis bending strength of double angle beams, 38 (1) (1996) 23–40.

[3] K.J.R. Rasmussen, Design of angle columns with locally unstable legs, J. Struct. Eng. (ASCE) 131 (10) (2005) 1553–1560.

[4] E. Ellobody, B. Young, Behavior of cold-formed steel plain angle columns, J. Struct. Eng. (ASCE) 131 (3) (2005) 457–466.

[5] N. Silvestre, P.B. Dinis, D. Camotim, Developments on the design of cold-formed steel angles, J. Struct. Eng. (ASCE) 139 (5) (2013) 680–694.

[6] A. Landesmann, D. Camotim, P.B. Dinis, R. Cruz. Short-to-intermediate slender pin-ended cold-formed steel equal-leg angle columns: Experimental investigation, numerical simulations and DSM design. Engineering Structures, 132 (2017):471–493.

[7] P.B. Dinis, D. Camotim, N. Silvestre, On the mechanics of thin-walled angle column instability, Thin-Walled Struct. 52 (2012) 80–89.

[8] B. Young, Tests and design of fixed-ended cold-formed steel plain angle columns, J. Struct. Eng. (ASCE) 130 (12) (2004) 1931–1940.

[9] P.B. Dinis, D. Camotim, N. Silvestre, On the mechanics of thin-walled angle column instability, Thin-Walled Struct. 52 (2012) 80–89.

[10] H. Kuwamura, Local buckling of thin-walled stainless steel members, Steel Struct. 3 (2003) 191–201.

[11] M. Theofanous, A. Liew, L. Gardner, Experimental study of stainless steel angles and channels in bending, Structures 4 (2015) 80–90.

[12] Y. Liang, V.V.K. Jeyapragasam, L. Zhang, O. Zhao, Flexural-torsional buckling behaviour of fixed-ended hot-rolled austenitic stainless steel equal-leg angle columns, J. Constr. Steel Res. 154 (2019) 43–54.

[13] A.A. de Menezes, P.C.G. da S. Vellasco, L.R.O. de Lima, A.T. da Silva, Experimental and numerical investigation of austenitic stainless steel hot-rolled angles under compression, J. Constr. Steel Res. 152 (2019) 42–56.

[14] L. Zhang, K.H. Tan, O. Zhao, Experimental and numerical studies of fixed-ended cold-formed stainless steel equal-leg angle section columns, Eng. Struct. 184 (2019) 134–144.

[15] EN 1993-1-4:2006 + A1:2015, Eurocode 3: Design of steel structures - Part 1-4: General rules - Supplementary rules for stainless steels, including amendment A1 (2015), Brussels, European Committee for Standardization (CEN), 2015.

[16] S. Afshan, L. Gardner, The continuous strength method for structural stainless steel design, Thin-Walled Struct. 68 (2013) 42–49.

[17] O. Zhao, S. Afshan, L. Gardner, Structural response and continuous strength method design of slender stainless steel cross-sections, Eng. Struct. 140 (2017) 14–25.

[18] O. Zhao, L. Gardner, The continuous strength method for the design of mono-symmetric and asymmetric stainless steel cross-sections in bending, J. Constr. Steel Res. 150 (2018) 141–152.

[19] EN ISO 6892-1: 2016, Metallic materials: tensile testing – Part 1 : Method of test at room temperature, Brussels: European Committee for Standardization (CEN), 2016.

[20] W. Ramberg, W.R. Osgood, Description of stress-strain curves by three parameters, National Advisory Committee for Aeronautics (NACA), technical note no. 902 (1943), Washington.

[21] H.N. Hill, Determination of stress-strain relations from offset yield strength values, National Advisory Committee for Aeronautics (NACA), technical note no. 927 (1944), Washington.

[22] E. Mirambell, E. Real, On the calculation of deflections in structural stainless steel beams: an experimental and numerical investigation, J. Constr. Steel Res. 54 (1) (2000) 109–133.

[23] K.J.R. Rasmussen, Full-range stress-strain curves for stainless steel alloys, J. Constr. Steel Res. 59 (1) (2003) 47–61.

[24] I. Arrayago, E. Real, L. Gardner, Description of stress–strain curves for stainless steel alloys, Mater. Des. 87 (2015) 540–552.

[25] B.W. Schafer, T. Peköz, Computational modeling of cold-formed steel: characterizing geometric imperfections and residual stresses, J. Constr. Steel Res. 47 (3) (1998) 193–210.

[26] M.T. Chen, B. Young, Material properties and structural behavior of cold-formed steel elliptical hollow section stub columns, Thin-Walled Struct. 134 (2019) 111–126.

[27] M.T. Chen, B. Young, Cross-sectional behavior of cold-formed steel semi-oval hollow sections, Eng. Struct. 177 (2018) 318–330.

[28] I. Arrayago, E. Real, Experimental study on ferritic stainless steel RHS and SHS cross-sectional resistance under combined loading, Structures 4 (2015) 69–79.

[29] R.D. Ziemiam, Guide to stability design criteria for metal structures, 6th ed., John Wiley & Sons, (2010).

[30] Centre for Advanced Structural Engineering, Compression tests of stainless steel tubular columns, Investigation report S770, University of Sydney, (1990).

[31] Hibbitt, Karlsson & Sorensen, Inc. ABAQUS/Standard user's Manual Volumes I-III and ABAQUS CAE Manual, Version 6.14, Pawtucket (USA); (2014).

[32] Y. Liang, O. Zhao, Y. Long, L. Gardner, Stainless steel channel sections under combined compression and minor axis bending – Part 1: Experimental study and numerical modelling, J. Constr. Steel Res. 152 (2019) 154–161.

[33] S. Niu, K.J.R. Rasmussen, F. Fan, Distortional-global interaction buckling of stainless steel C-beams : Part II – Numerical study and design, J. Constr. Steel Res. 96 (2014) 40–53.

[34] Y. Sun, O. Zhao, Material response and local stability of high-chromium stainless steel welded I-sections, Eng. Struct. 178 (2019) 212–226.

[35] N. Silvestre, D. Camotim, P.B. Dinis, Post-buckling behaviour and direct strength design of lipped channel columns experiencing local/distortional interaction, J. Constr. Steel Res. 73 (2012) 12–30.

[36] L. Gardner, N. Saari, F. Wang, Comparative experimental study of hot-rolled and cold-formed rectangular hollow sections, Thin-Walled Struct. 48 (7) (2010) 495–507.

[37] J. Szalai, F. Papp, A new residual stress distribution for hot-rolled I-shaped sections, J. Constr. Steel Res. 61 (6) (2005) 845–861.

[38] T.M. Chan, L. Gardner, Compressive resistance of hot-rolled elliptical hollow sections,

Eng. Struct. 30 (2008) 522–832.

[39] M. Ashraf, L. Gardner, D.A. Nethercot, Finite element modelling of structural stainless steel cross-sections, Thin-Walled Struct. 44 (2006) 1048–1062.

[40] E. Ellobody, B. Young, Structural performance of cold-formed high strength stainless steel columns, J. Constr. Steel Res. 61 (2005) 1631–1649.

[41] N. Saliba, L. Gardner, Cross-section stability of lean duplex stainless steel welded I-sections, J. Constr. Steel Res. 80 (2013) 1–14.

[42] P.B. Dinis, D. Camotim, A novel DSM-based approach for the rational design of fixed-ended and pin-ended short-to-intermediate thin-walled angle columns. Thin-Walled Struct. 87 (2015) 158–182.

[43] I. Arrayago, K.J.R. Rasmussen, E. Real, Full slenderness range DSM approach for stainless steel hollow cross-section columns and beam-columns, J. Constr. Steel Res. 138 (2017) 246–263.

[44] O. Zhao, L. Gardner, B. Young, Buckling of ferritic stainless steel members under combined axial compression and bending, J. Constr. Steel Res. 117 (2016) 35–48.

[45] O. Zhao, L. Gardner, B. Young, Structural performance of stainless steel circular hollow sections under combined axial load and bending – Part 1: Experiments and numerical modelling, Thin-Walled Struct. 101 (2016) 231–239.

[46] M.T. Chen, B. Young, Behavior of cold-formed steel elliptical hollow sections subjected to bending, J. Constr. Steel Res. 158 (2019) 317–330.

[47] B.W. Schafer, S. Ádány, Buckling analysis of cold-formed steel members using CUFSM: conventional and constrained finite strip method, 18th Int. Spec. Conf. Cold-Formed

Steel Struct. (2006).

[48] C. Buchanan, L. Gardner, A. Liew, The continuous strength method for the design of circular hollow sections, J. Constr. Steel Res. 118 (2016) 207–216.

Table 1

Summary of key measured material properties from the tensile coupon tests.

Section identifier	Cross-section	Grade	E (GPa)	$\sigma_{0.2}$ (MPa)	$\sigma_{1.0}$ (MPa)	σ_u (MPa)	ε_u (%)	ε_f (%)	R-O exponents n	$n'_{0.2,1.0}$
A1	A 80×10	1.4307	202	342	395	685	38	71	8.3	1.8
A2	A 80×10	1.4404	189	438	477	716	36	52	9.3	2.5
A3	A 80×10	1.4571	188	471	515	663	31	50	9.3	2.5
A4	A 100×10	1.4307	205	331	383	687	54	70	16.0	1.7
A5	A 100×8	1.4571	193	404	465	642	36	49	7.6	2.7

Table 2

Measured geometric properties of the tested hot-rolled austenitic stainless steel equal-leg angle section stub columns and beams.

Cross-section	Grade	Specimen ID	L (mm)	b (mm)	t (mm)	$\omega_{\max,1}$ (mm)	$\omega_{\max,2}$ (mm)	ω_0 (mm)
A 80×10	1.4307	A1-S1	239.7	80.41	9.44	0.07	0.06	0.07
		A1-S2	240.3	80.20	9.43	0.09	0.09	0.09
		A1-B1	1600.0	81.31	9.42	0.13	0.19	0.19
		A1-B2	1600.0	81.38	9.45	0.18	0.17	0.18
A 80×10	1.4404	A2-S1	239.5	79.05	9.52	0.16	0.20	0.20
		A2-S2	240.0	78.67	9.52	0.22	0.13	0.22
		A2-B1	1600.0	80.46	9.56	0.12	0.09	0.12
		A2-B2	1600.0	80.44	9.55	0.12	0.07	0.12
A 80×10	1.4571	A3-S1	240.5	78.55	9.24	0.08	0.09	0.09
		A3-S2	240.0	78.86	9.37	0.11	0.11	0.11
		A3-B1	1600.0	80.42	9.56	0.37	0.24	0.37
		A3-B2	1600.0	80.43	9.54	0.29	0.14	0.29
A 100×10	1.4307	A4-S1	300.5	98.96	9.83	0.15	0.09	0.15
		A4-S2	300.2	99.39	9.75	0.10	0.13	0.13
		A4-B1	1600.0	99.55	9.86	0.30	0.18	0.30
		A4-B2	1600.0	99.72	9.80	0.25	0.31	0.31
A 100×8	1.4571	A5-S1	300.4	99.67	7.89	0.09	0.05	0.09
		A5-S2	300.4	99.87	7.88	0.11	0.13	0.13
		A5-B1	1600.0	100.07	7.91	0.11	0.08	0.11
		A5-B2	1600.0	100.11	7.89	0.13	0.11	0.13

Table 3

Test results for the stub column specimens.

Specimen ID	Cross-section class (EC3)	$\bar{\lambda}_p$	N_u (kN)	δ_0 (mm)	$N_u/(A\sigma_{0.2})$	$N_u/N_{u,EC3}$	$N_u/N_{u,csm}$
A1-S1	Class 3	0.47	584.7	3.8	1.20	1.20	1.13
A1-S2	Class 3	0.47	550.7	3.1	1.13	1.13	1.06
A2-S1	Class 4	0.53	694.7	2.2	0.93	1.12	1.08
A2-S2	Class 4	0.53	664.2	2.2	0.89	1.08	1.05
A3-S1	Class 4	0.57	678.5	2.4	1.05	1.05	1.03
A3-S2	Class 4	0.56	681.8	2.5	1.04	1.04	1.02
A4-S1	Class 4	0.59	669.5	2.5	1.09	1.09	1.08
A4-S2	Class 4	0.57	696.1	2.5	1.14	1.14	1.12
A5-S1	Class 4	0.78	663.2	0.9	1.25	1.25	1.07
A5-S2	Class 4	0.78	641.7	0.9	1.20	1.20	1.03
					Mean	1.13	1.07
					COV	0.07	0.04

Table 4

Test results for the laterally restrained beam specimens.

Specimen ID	Cross-section class (EC3)	$\bar{\lambda}_p$	M_u (kNm)	M_u/M_{pl}	M_u/M_{el}	R	$M_u/M_{u,EC3}$	$M_u/M_{u,csm}$
A1-B1	Class 3	0.36	9.87	1.02	1.84	>2.21	1.84	1.15
A1-B2	Class 3	0.36	9.87	1.03	1.86	>2.21	1.86	1.16
A2-B1	Class 3	0.41	15.54	1.28	2.30	>2.14	2.30	1.27
A2-B2	Class 3	0.41	15.54	1.28	2.31	>2.14	2.31	1.28
A3-B1	Class 3	0.42	13.35	1.02	1.85	2.24	1.85	1.15
A3-B2	Class 3	0.43	13.35	1.02	1.84	2.24	1.84	1.15
A4-B1	Class 3	0.41	15.58	1.07	1.92	2.79	1.92	1.20
A4-B2	Class 3	0.42	15.58	1.06	1.92	2.79	1.92	1.20
A5-B1	Class 4	0.60	16.65	1.12	2.02	>1.54	2.07	1.22
A5-B2	Class 4	0.60	16.65	1.12	2.02	>1.54	2.07	1.22
						Mean	2.00	1.20
						COV	0.18	0.05

Table 5

Comparison of stub column test results with FE results for various imperfection levels.

Specimen ID	Finite element N_u / Test N_u				
	Measured value ω_0	$t/10$	$t/20$	$t/50$	$t/100$
A1-S1	0.98	0.88	0.91	0.95	0.97
A1-S2	1.04	0.93	0.97	1.01	1.03
A2-S1	1.02	0.96	0.99	1.02	1.04
A2-S2	1.05	0.99	1.02	1.06	1.08
A3-S1	1.00	0.93	0.96	0.99	1.00
A3-S2	0.99	0.92	0.95	0.98	1.00
A4-S1	1.01	0.92	0.96	0.99	1.02
A4-S2	0.97	0.89	0.92	0.96	0.98
A5-S1	0.99	0.90	0.94	0.97	0.99
A5-S2	1.02	0.93	0.96	1.00	1.02
Mean	1.00	0.93	0.96	0.99	1.01
COV	0.02	0.03	0.03	0.03	0.03

Table 6

Comparison of laterally restrained beam test results with FE results for various imperfection levels.

Specimen ID	Finite element M_u / Test M_u				
	Measured value ω_0	$t/10$	$t/20$	$t/50$	$t/100$
A1-B1	0.96	0.90	0.94	0.96	0.98
A1-B2	0.97	0.90	0.94	0.96	0.98
A2-B1	1.03	0.92	0.97	1.00	1.03
A2-B2	1.03	0.92	0.97	1.00	1.03
A3-B1	0.92	0.84	0.92	0.95	0.98
A3-B2	0.94	0.84	0.92	0.95	0.98
A4-B1	0.99	0.97	0.99	1.01	1.03
A4-B2	0.99	0.97	0.99	1.01	1.03
A5-B1	1.02	0.93	0.95	0.99	1.04
A5-B2	1.01	0.93	0.95	0.99	1.04
Mean	0.98	0.91	0.96	0.98	1.02
COV	0.03	0.04	0.03	0.03	0.03

Table 7

Comparison of test and FE results with EC3 and CSM design resistances for stub columns and laterally restrained beams.

Specimen type	Cross-section type*	No. of test data	No. of FE data	$N_u/N_{u,EC3}$ or $M_u/M_{u,EC3}$		$N_u/N_{u,csm}$ or $M_u/M_{u,csm}$	
				Mean	COV	Mean	COV
Stub columns	Non-slender section	8	28	1.18	0.06	1.11	0.02
	Slender section	2	22	1.24	0.18	1.06	0.03
	Total	10	50	1.21	0.14	1.09	0.03
Laterally restrained beams	Non-slender section	10	26	1.84	0.25	1.18	0.05
	Slender section	0	22	1.78	0.02	1.05	0.01
	Total	10	48	1.81	0.21	1.13	0.08

* The cross-section type is defined according to EN 1993-1-4.

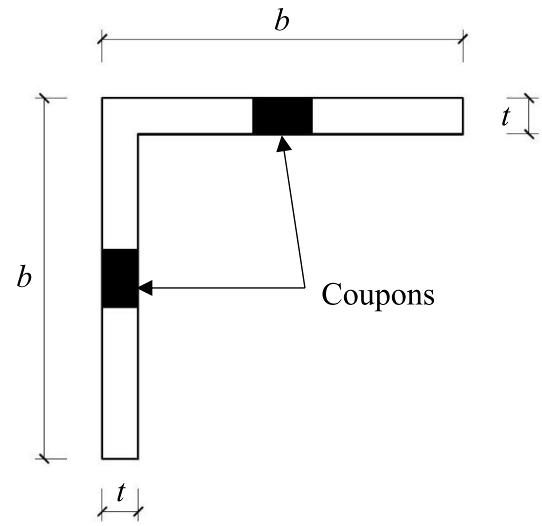

Fig. 1. Locations of coupons in angle sections.

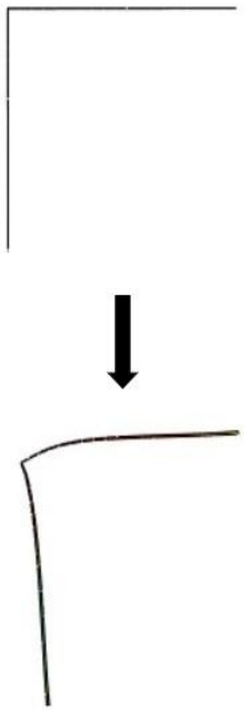

(a) Schematic failure mode of stub column.

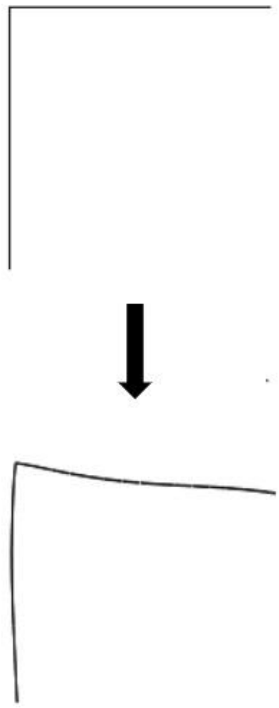

(b) Schematic failure mode of laterally restrained beam.

(c) Rig for local geometric imperfection measurements.

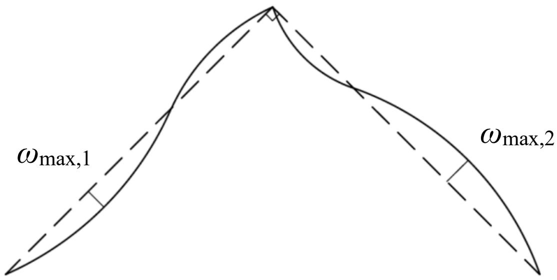

(d) Schematic diagram of initial local imperfection of angle section.

Fig. 2. Initial local geometric imperfection measurement.

Fig. 3. Equal-leg angle stub column test rig.

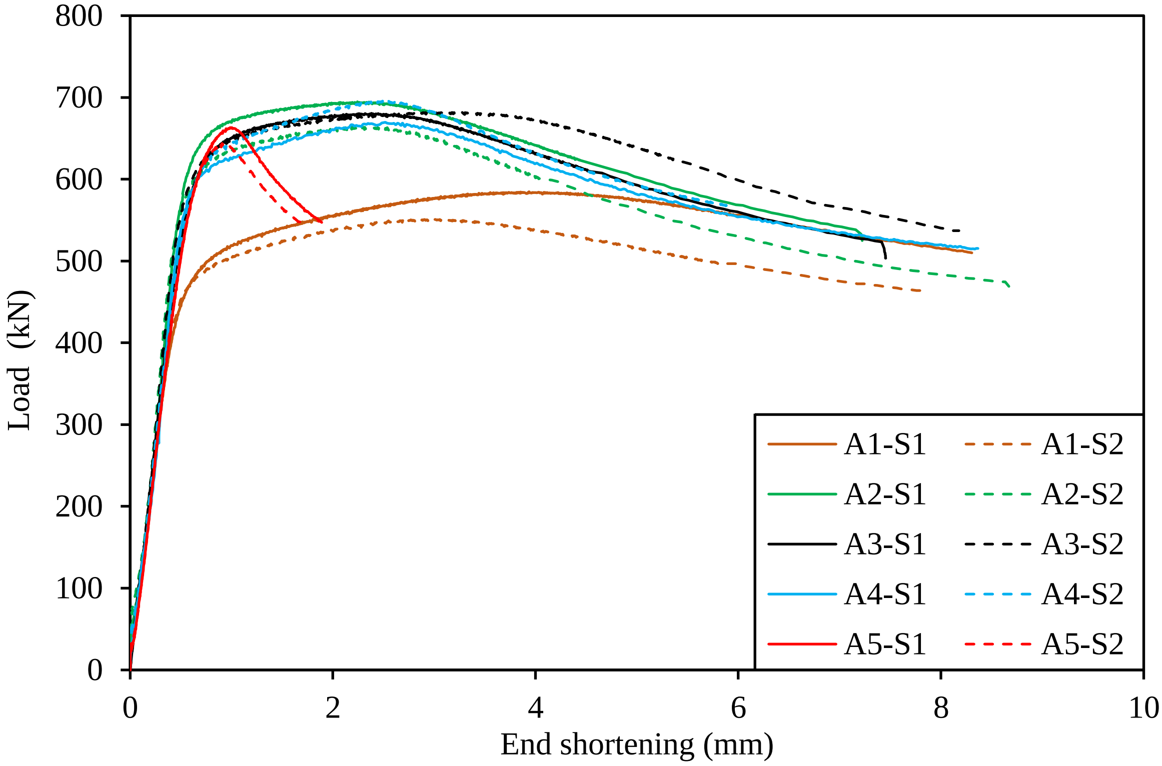

Fig. 4. Load–end shortening curves of the tested stub columns.

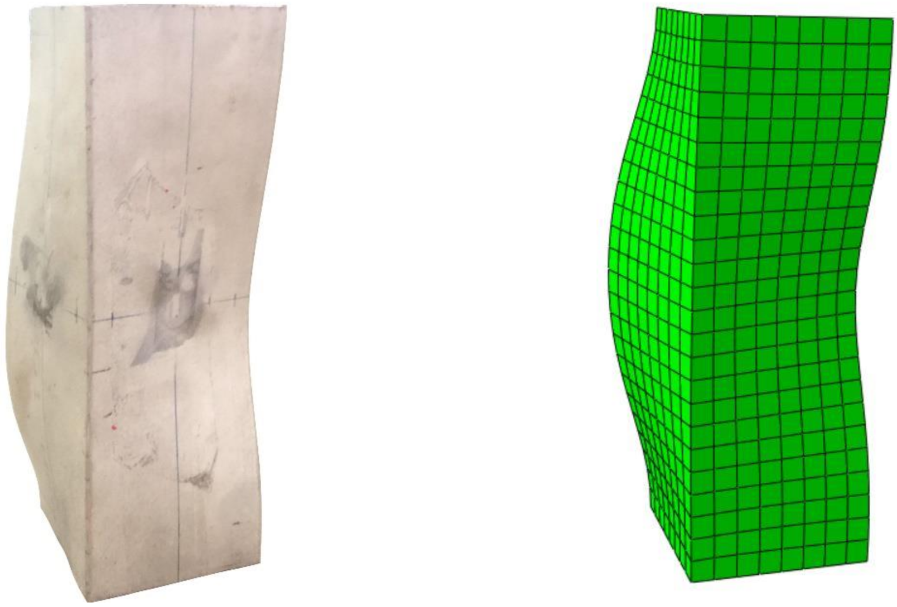

Fig. 5. Test and FE failure modes for stub column specimen A3-S1.

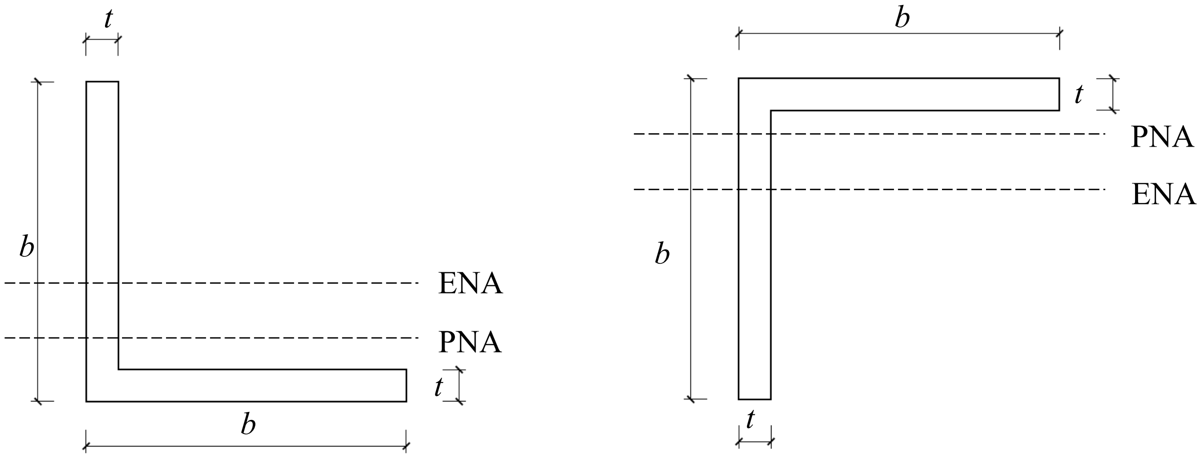

(a) In the 'L' orientation

(b) In the 'reverse L' orientation

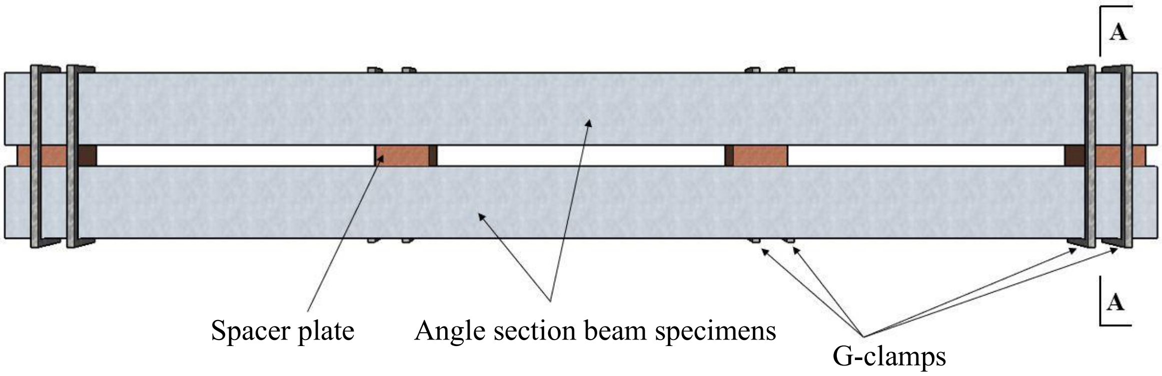

(a) Top view.

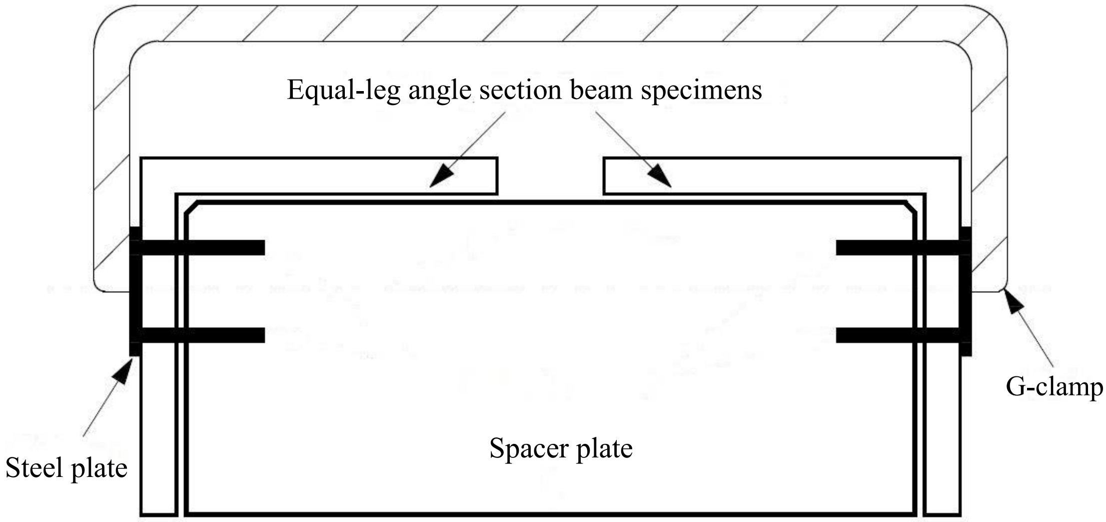

(b) Side view (A-A).

Fig. 7. Schematic diagram of two equal-leg angle section beams tested in pair.

Fig. 8. Test rig for laterally restrained double-angle beams bent about the geometric axes in the 'reverse L' orientation.

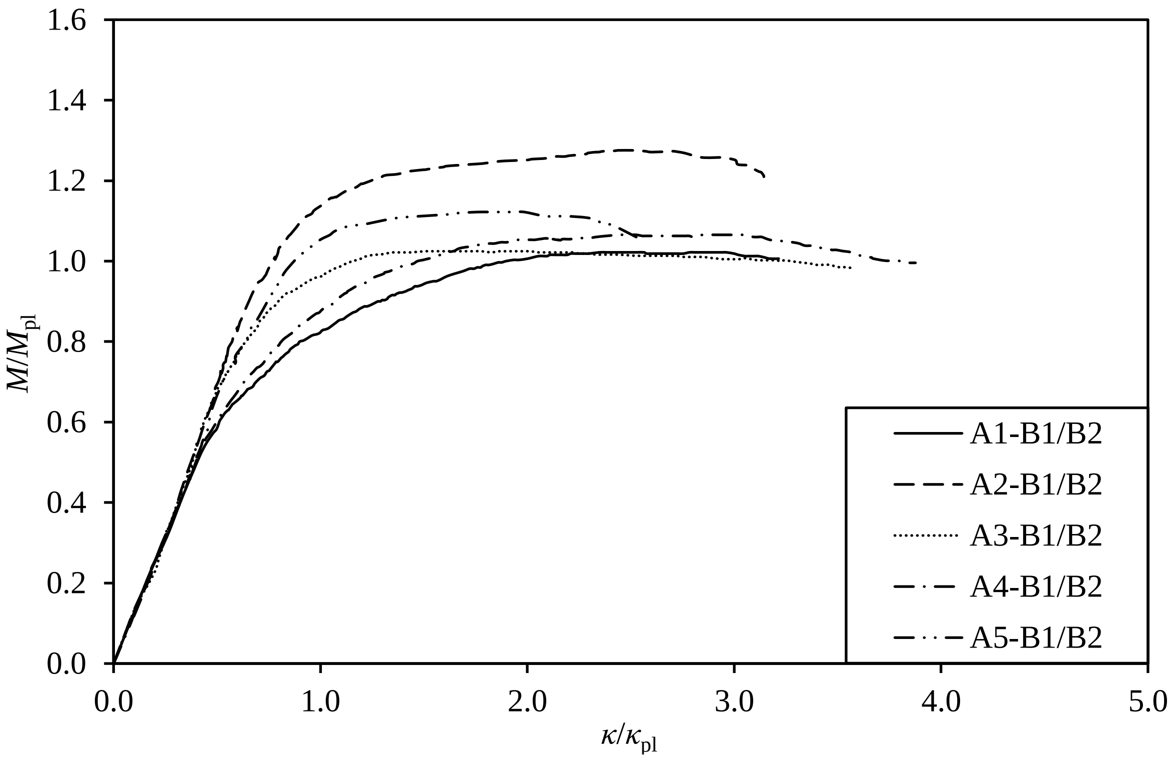

Fig. 9. Normalised moment–curvatures of the laterally restrained beam specimens.

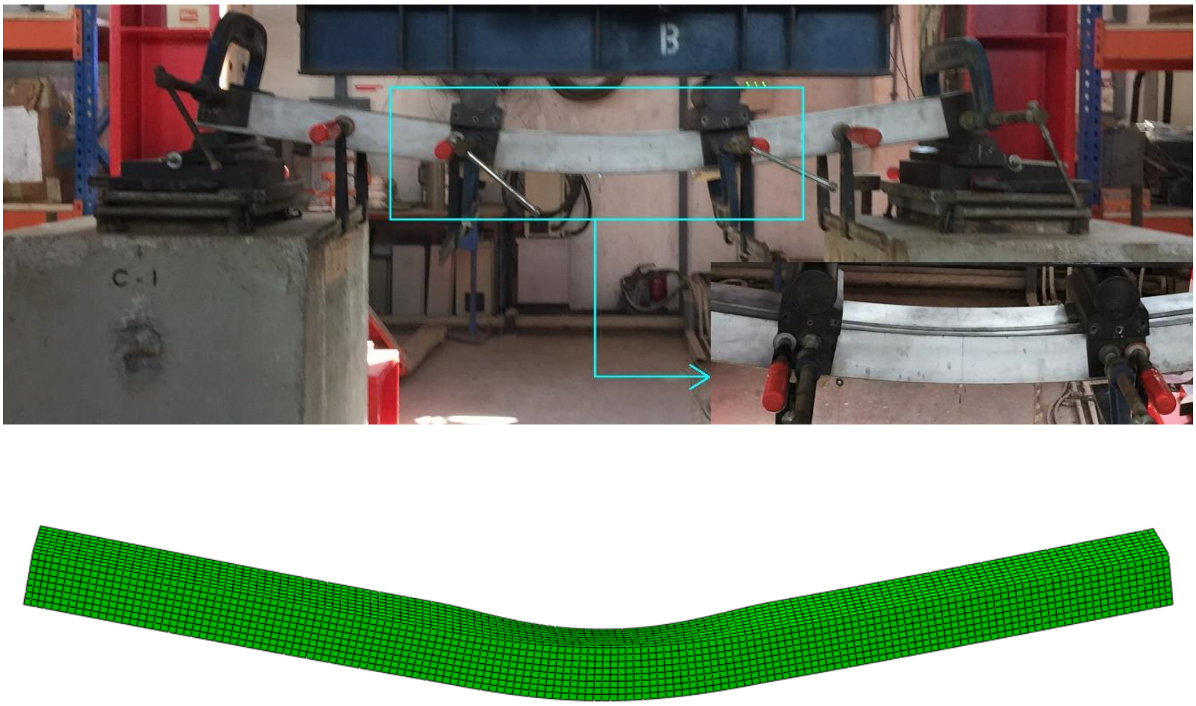

Fig. 10. Test and FE failure modes for beam specimen A1-B1 (or A1-B2).

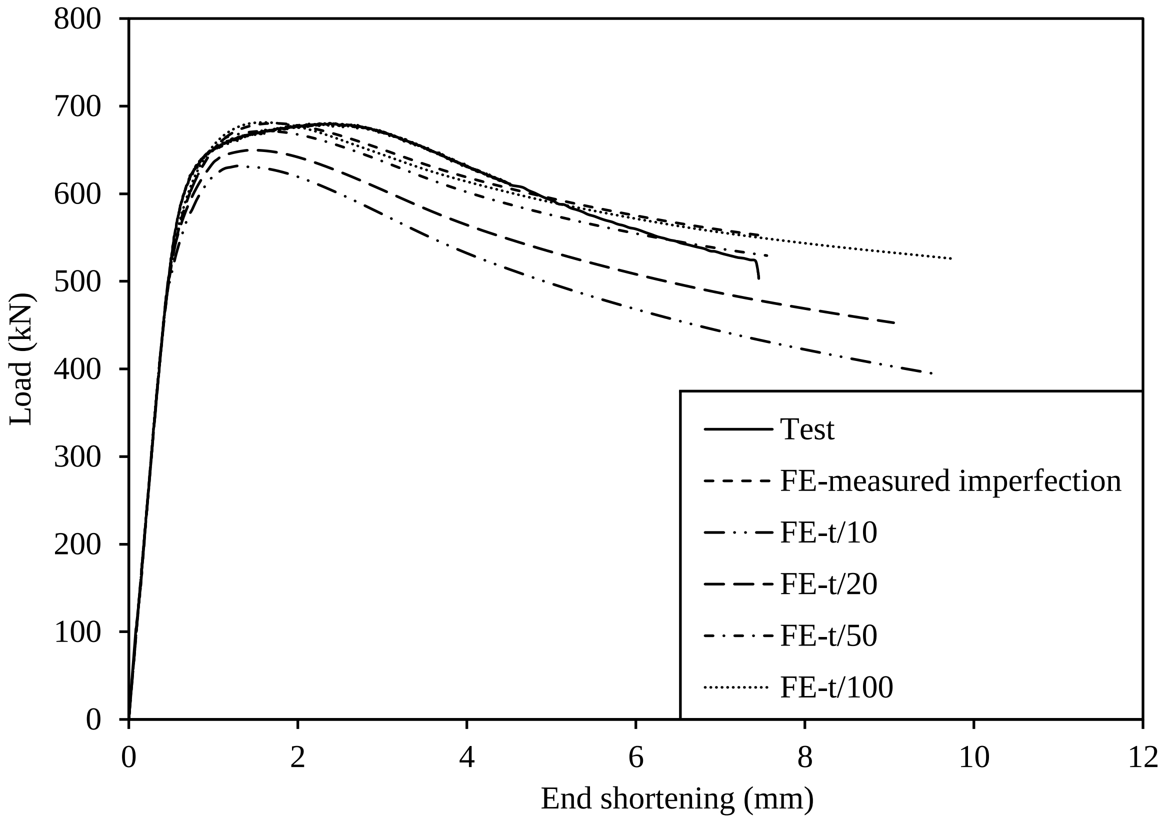

(a) Stub column specimen A3-S1.

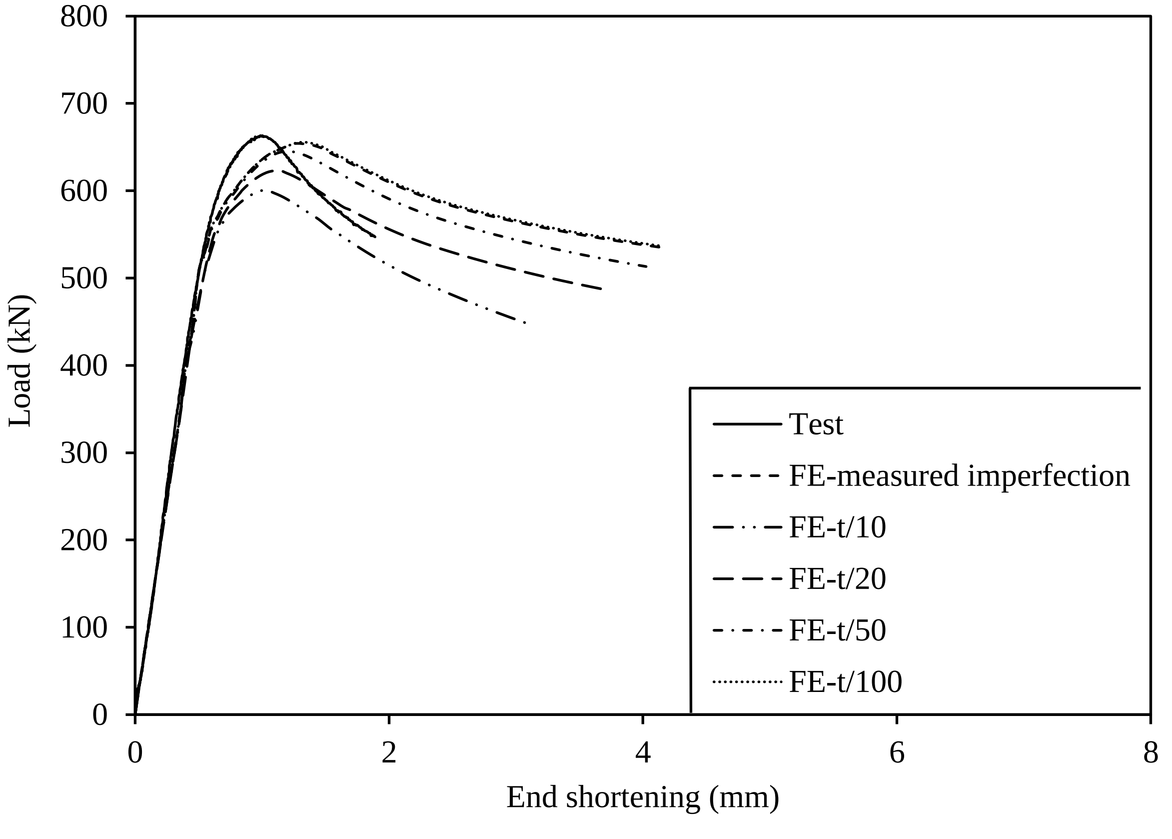

(b) Stub column specimen A5-S1.

Fig. 11. Test and FE load–end shortening curves.

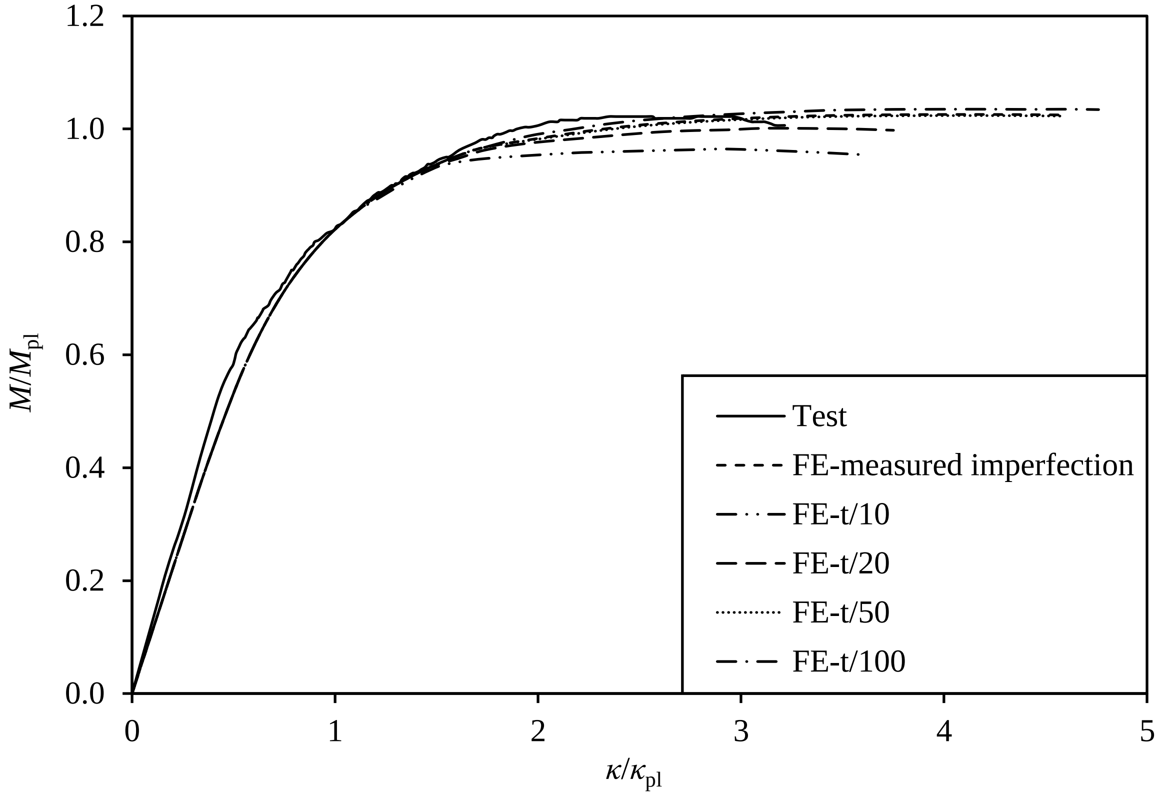

(a) Beam specimen A1-B1.

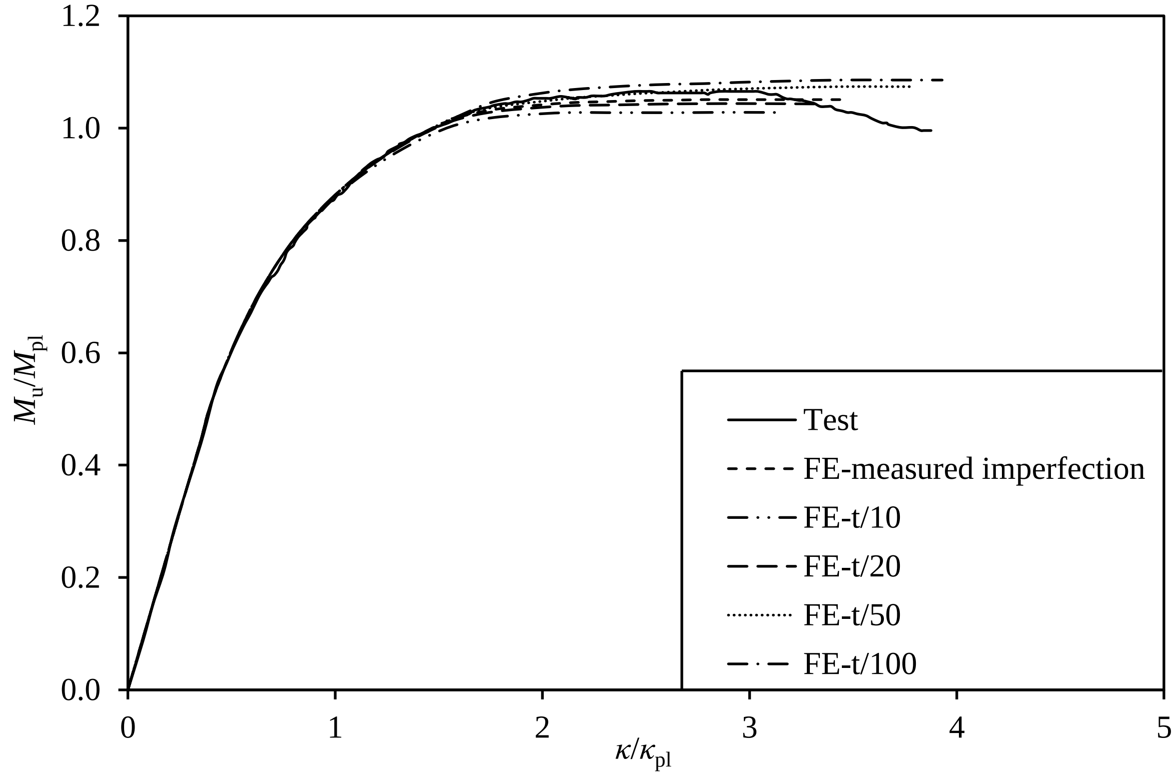

(b) Beam specimen A4-B1.

Fig. 12. Test and FE normalised moment–curvature curves.

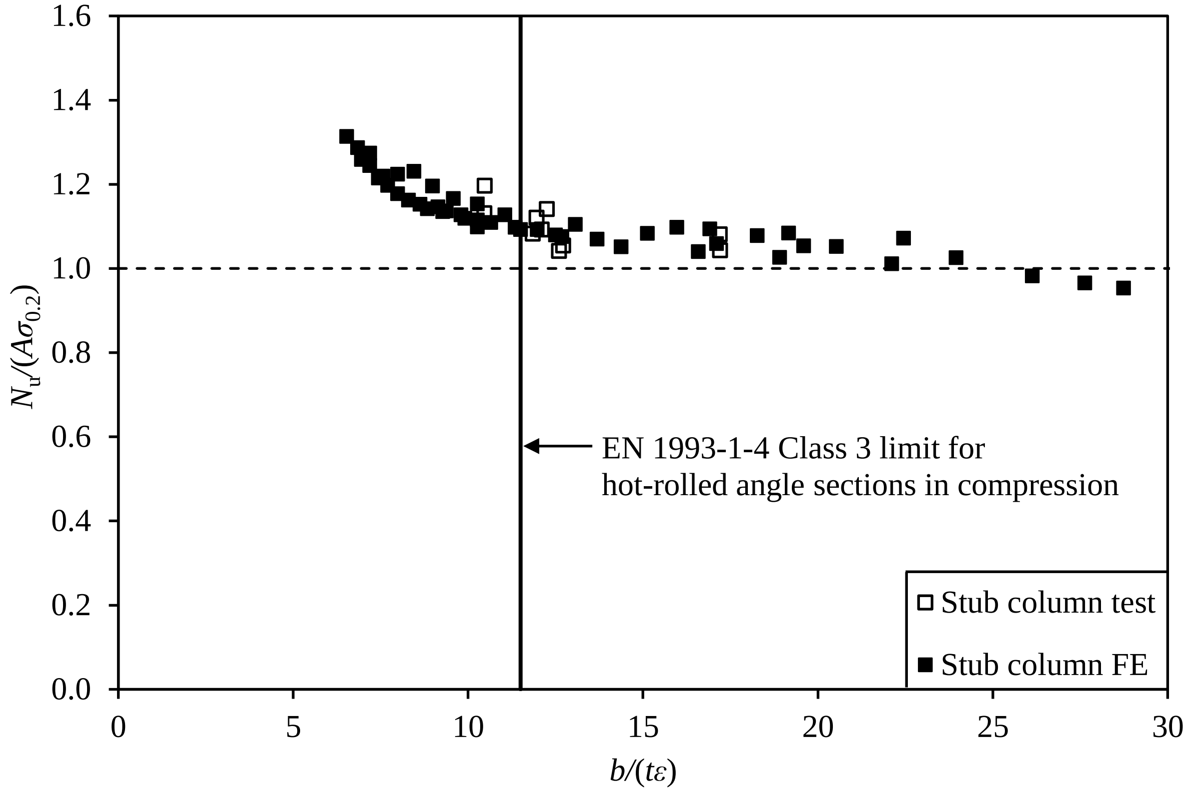

Fig. 13. EC3 Class 3 limit for stainless steel equal-leg angles under compression.

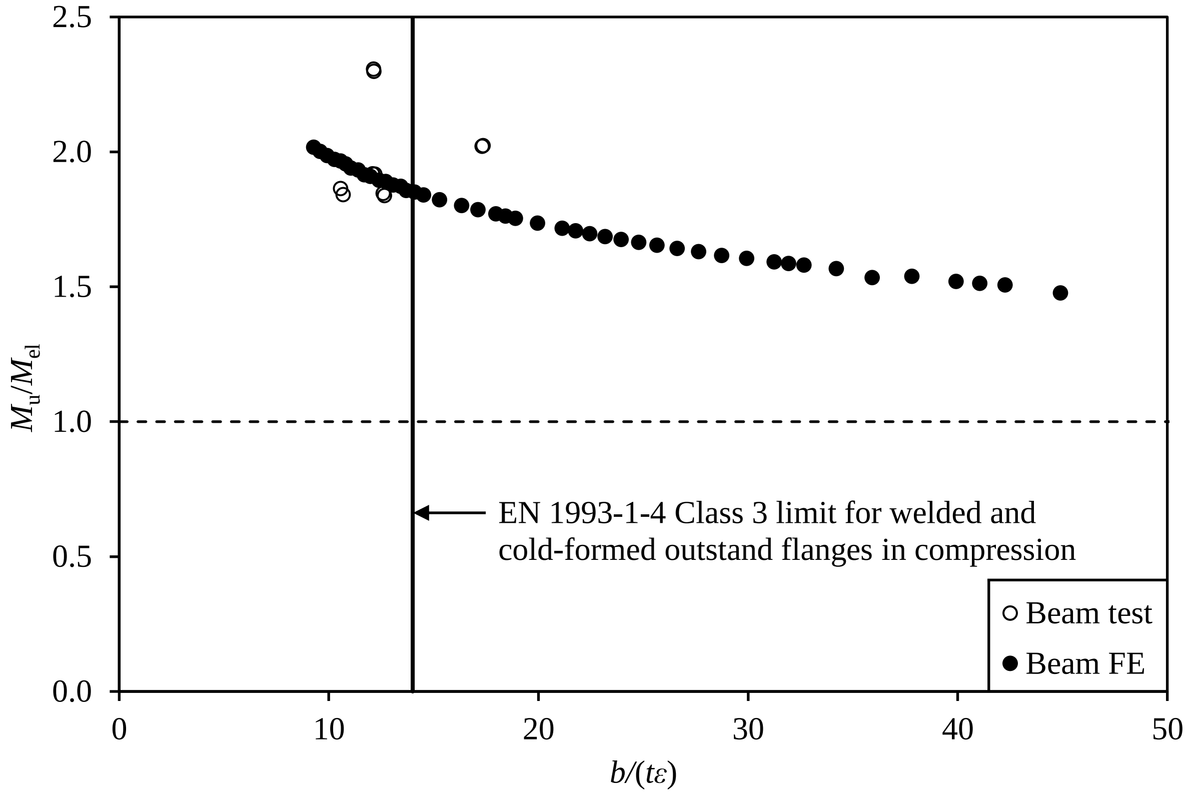

Fig. 14. EC3 Class 3 limit for stainless steel equal-leg angles in geometric axis bending.

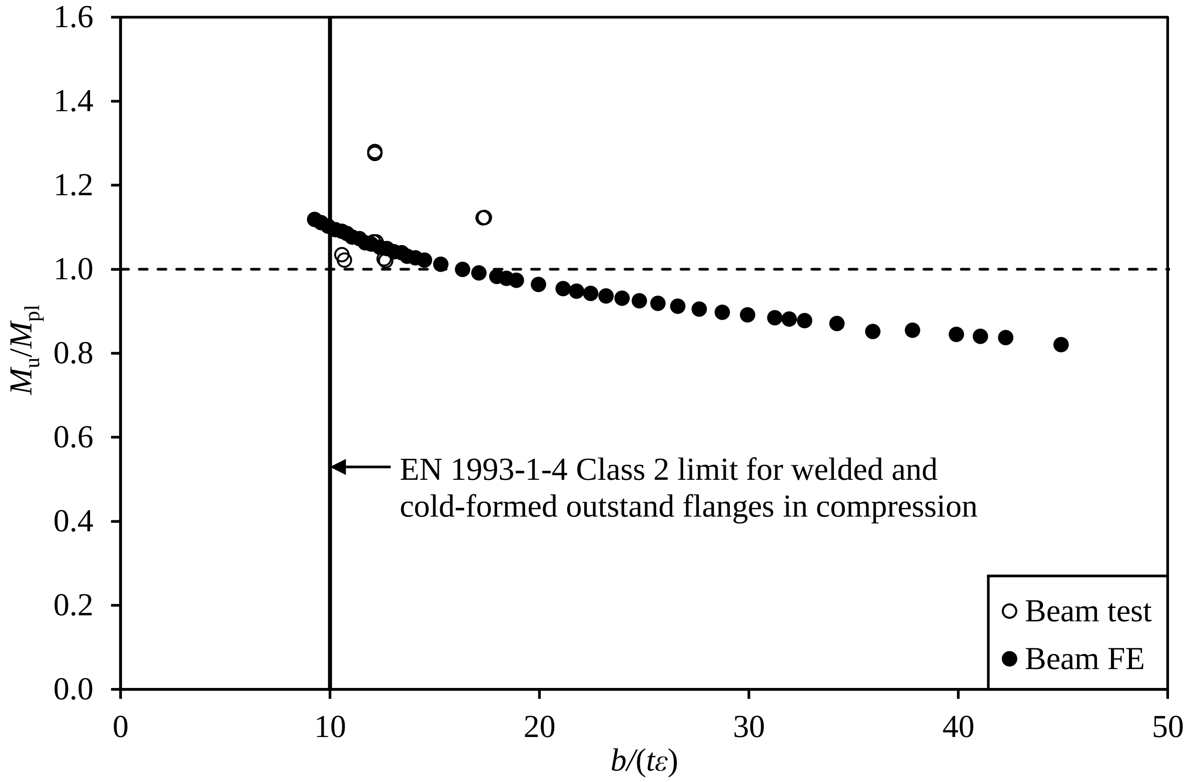

Fig. 15. EC3 Class 2 limit for equal-leg angles in geometric axis bending.

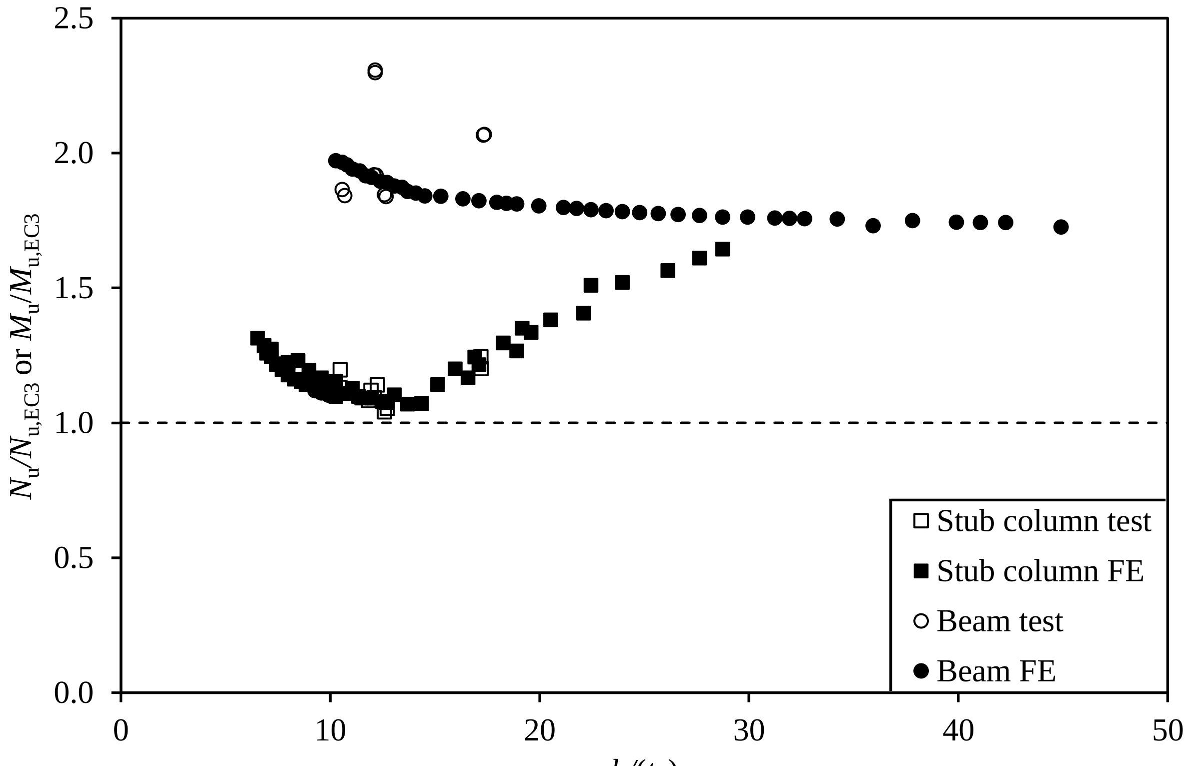

Fig. 16. Comparison of test and FE results with EN 1993-1-4 resistance predictions.

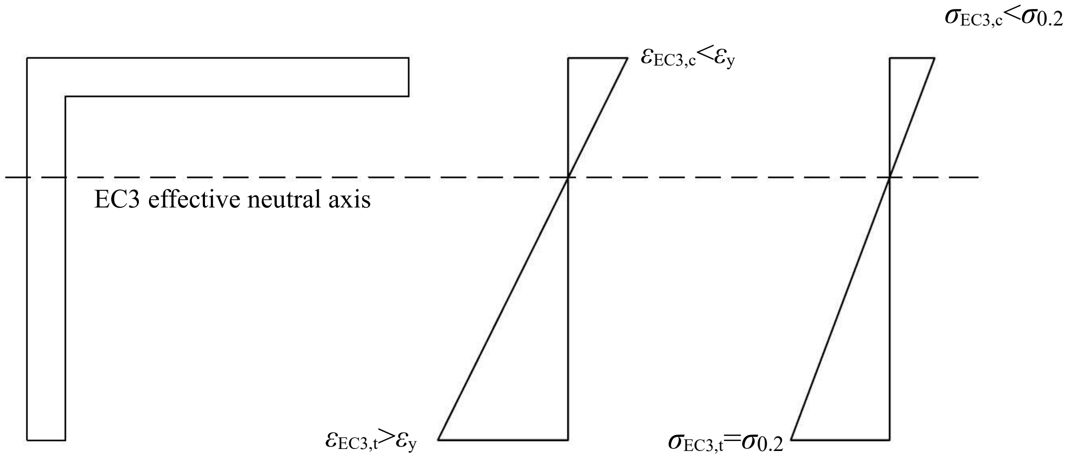

Fig. 17. EC3 design strain and stress distributions. ($\varepsilon_{EC3,c}$ and $\varepsilon_{EC3,t}$ are the EC3 design strains at the extreme compressive and tensile fibres, respectively, while $\sigma_{EC3,c}$ and $\sigma_{EC3,t}$ are the corresponding EC3 design stresses.)

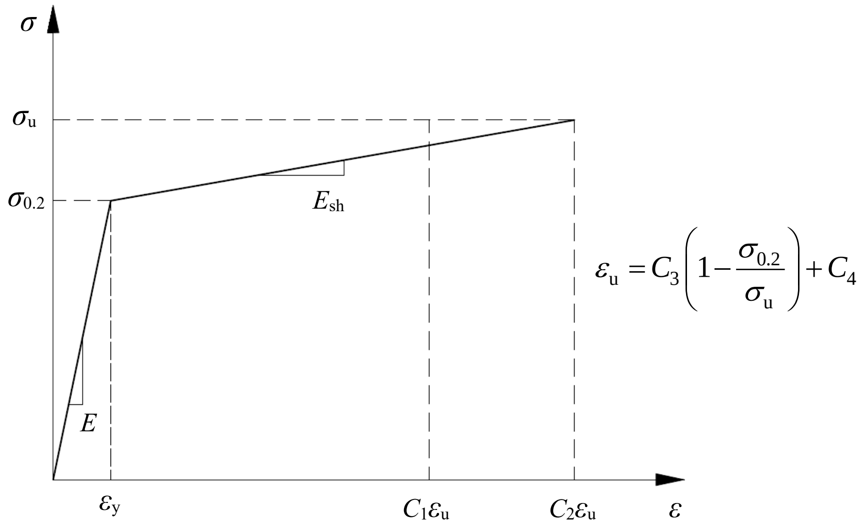

Fig. 18. CSM elastic, linear hardening material model.

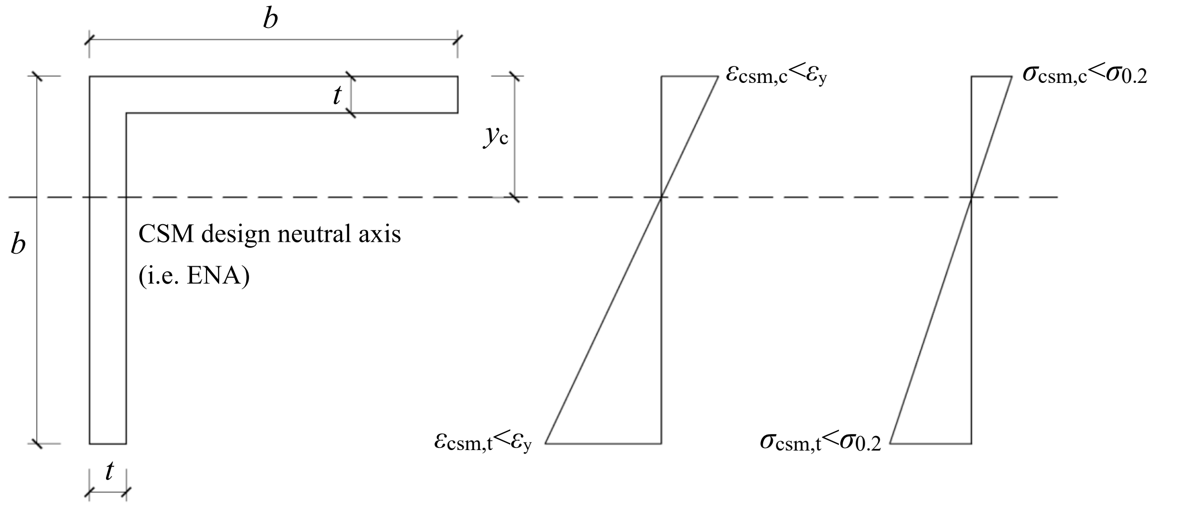

(a) Angle section with $\varepsilon_{csm,c}<\varepsilon_y$ and $\varepsilon_{csm,t}<\varepsilon_y$ (i.e. $\varepsilon_{csm,d}<\varepsilon_y$).

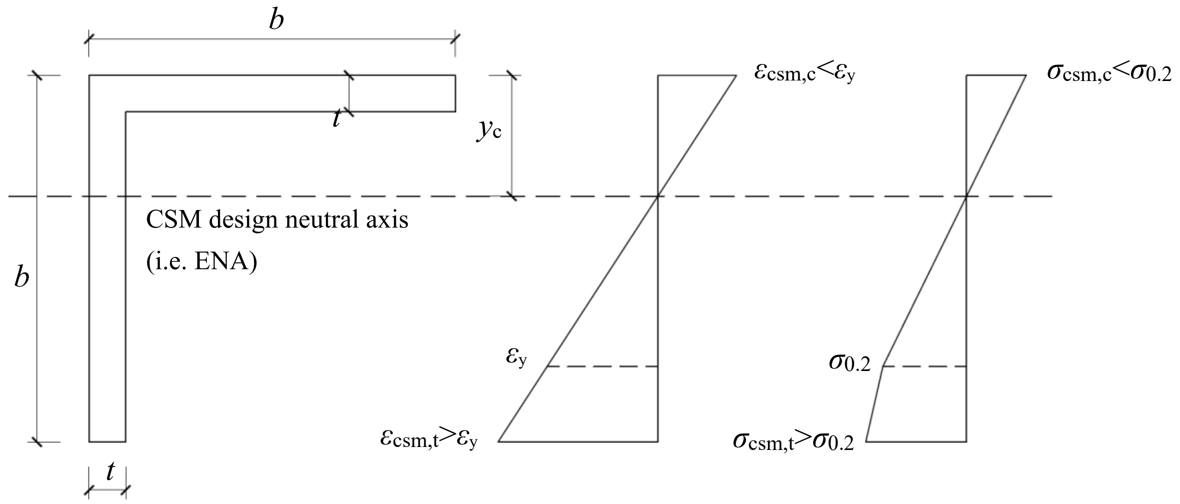

(b) Angle section with $\varepsilon_{csm,c}<\varepsilon_y$ but $\varepsilon_{csm,t}>\varepsilon_y$ (i.e. $\varepsilon_{csm,d}>\varepsilon_y$).

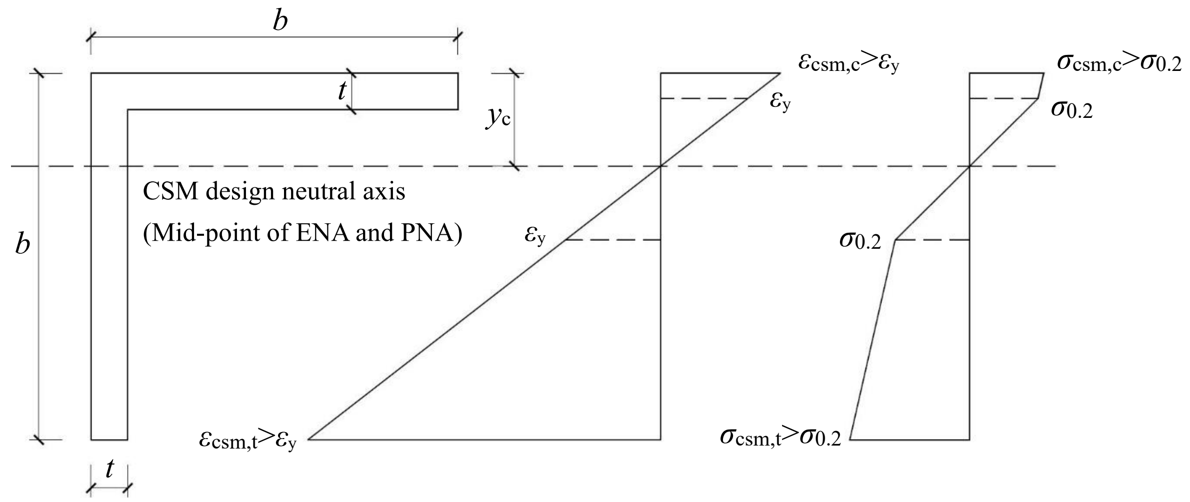

(c) Angle section with $\varepsilon_{csm,c}>\varepsilon_y$ and $\varepsilon_{csm,t}>\varepsilon_y$ (i.e. $\varepsilon_{csm,d}>\varepsilon_y$).

Fig. 19. CSM design strain and stress distributions. ($\sigma_{csm,c}$ and $\sigma_{csm,t}$ are the CSM design stresses at the extreme compressive and tensile fibres, respectively.)

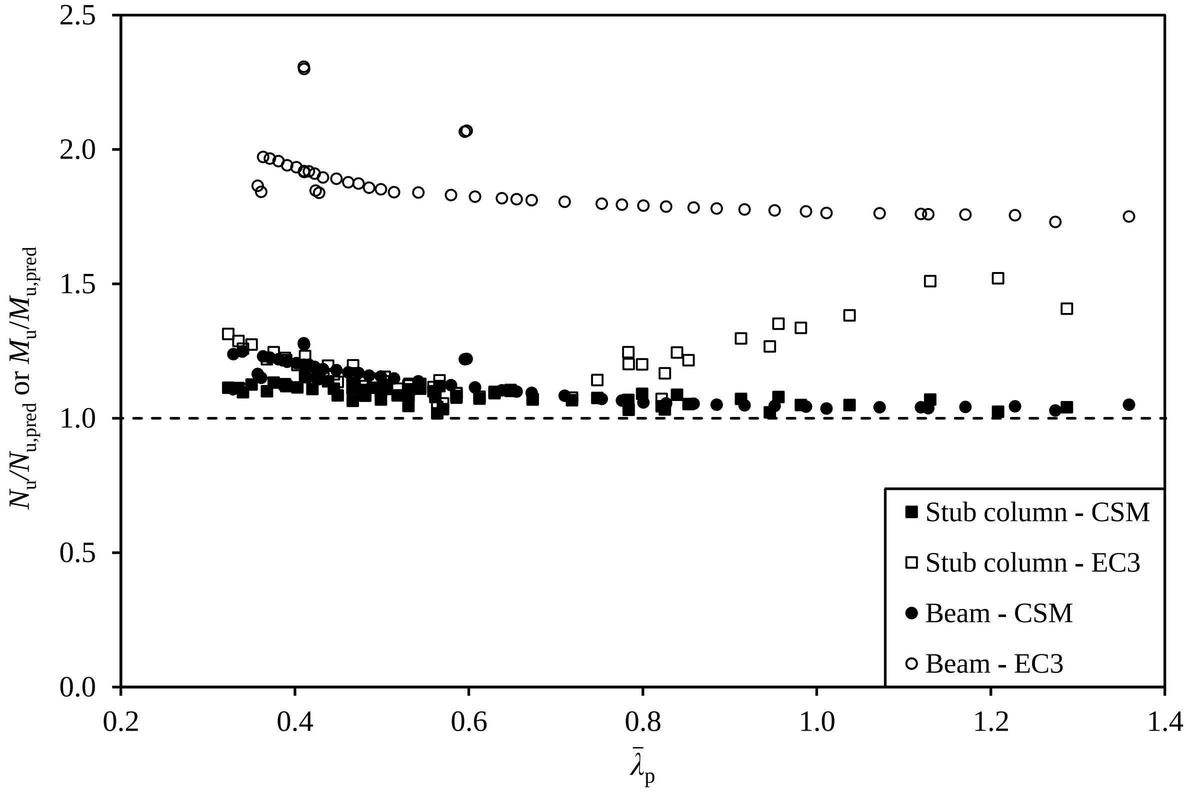

Fig. 20. Comparison of experimental and numerical results with CSM and EC3 resistance predictions.